# Removing the Effects of Tropical Dynamics from North Pacific Climate Variability

YINGYING ZHAO,[a,b] MATTHEW NEWMAN,[c,d] ANTONIETTA CAPOTONDI,[c,d] EMANUELE DI LORENZO,[a] AND DAOXUN SUN[a,b]

[a] *Program in Ocean Science and Engineering, Georgia Institute of Technology, Atlanta, Georgia*
[b] *Pilot National Laboratory for Marine Science and Technology, Qingdao, China*
[c] *Climate Diagnostics Center, CIRES, University of Colorado at Boulder, Boulder, Colorado*
[d] *Physical Sciences Laboratory, NOAA, Boulder, Colorado*

(Manuscript received 30 April 2021, in final form 2 August 2021)

ABSTRACT: Teleconnections from the tropics energize variations of the North Pacific climate, but detailed diagnosis of this relationship has proven difficult. Simple univariate methods, such as regression on El Niño–Southern Oscillation (ENSO) indices, may be inadequate since the key dynamical processes involved—including ENSO diversity in the tropics, re-emergence of mixed layer thermal anomalies, and oceanic Rossby wave propagation in the North Pacific—have a variety of overlapping spatial and temporal scales. Here we use a multivariate linear inverse model to quantify tropical and extratropical multiscale dynamical contributions to North Pacific variability, in both observations and CMIP6 models. In observations, we find that the tropics are responsible for almost half of the seasonal variance, and almost three-quarters of the decadal variance, along the North American coast and within the Subtropical Front region northwest of Hawaii. SST anomalies that are generated by local dynamics within the northeast Pacific have much shorter time scales, consistent with transient weather forcing by Aleutian low anomalies. Variability within the Kuroshio–Oyashio Extension (KOE) region is considerably less impacted by the tropics, on all time scales. Consequently, without tropical forcing the dominant pattern of North Pacific variability would be a KOE pattern, rather than the Pacific decadal oscillation (PDO). In contrast to observations, most CMIP6 historical simulations produce North Pacific variability that maximizes in the KOE region, with amplitude significantly higher than observed. Correspondingly, the simulated North Pacific in all CMIP6 models is shown to be relatively insensitive to the tropics, with a dominant spatial pattern generally resembling the KOE pattern, not the PDO.

KEYWORDS: ENSO; Climate variability; Pacific decadal oscillation

## 1. Introduction

El Niño–Southern Oscillation (ENSO), the strongest signal in the tropical Pacific on seasonal-to-interannual time scales, drives atmospheric teleconnections that project tropical variability into the extratropics (''the atmospheric bridge''), significantly impacting the climate, weather, and ecosystems throughout the Pacific (e.g., Alexander 1992; Wang et al. 2000; Alexander et al. 2002; Vimont 2005; Di Lorenzo et al. 2010; Deser et al. 2012; Liu and Di Lorenzo 2018; Capotondi et al. 2020a). Consequently, ENSO impacts North Pacific sea surface temperature (SST) variability and, specifically, North Pacific climate ''modes'' of variability including the Pacific decadal oscillation (PDO) (e.g., Zhang et al. 1997; Newman et al. 2003; Vimont 2005) and the North Pacific Gyre Oscillation (NPGO) (Di Lorenzo et al. 2010).

Still, the extent of this ENSO impact throughout the North Pacific remains uncertain. Some studies have suggested that a simple reddening of ENSO, occurring as the North Pacific integrates the effects of ENSO teleconnections, may generate a substantial fraction of PDO variance (e.g., Newman et al. 2003; Schneider and Cornuelle 2005). More generally, the PDO appears to result from a combination of different dynamical processes, including ENSO teleconnections, local atmosphere–ocean interactions, and ocean dynamics (Newman et al. 2016). Others, however, have argued that most variability in the North Pacific is independent of ENSO. For example, Chen and Wallace (2016) performed a rotation of the two leading empirical orthogonal function (EOF) patterns of Pacific SST anomalies to yield two new orthogonal patterns, one that tracks ENSO but has only a weak North Pacific footprint, and a second that bears considerable similarity to the PDO pattern but is seemingly independent of ENSO. Wills et al. (2018) suggested that the observed interdecadal variability of a variant of the PDO, a new pattern identified with ''low-frequency component analysis,'' is nearly independent of ENSO.

Perhaps the most common approach for ''removing the ENSO signal'' is to linearly regress a variable against some ENSO index, and then subtract the regressed portion from that variable. This regression may be either simultaneous or at some fixed lag, and the ENSO indices may include the Southern Oscillation index, the Niño-3.4 index, or the principal component (PC) of the dominant EOF of tropical SST (e.g., Robock and Mao 1995; Kelly and Jones 1996; Cane et al. 1997; Angell 2000; Santer et al. 2001; Chiang and Vimont 2004; Wheeler and Hendon 2004; Thompson et al. 2008, 2009; Vyushin and Kushner 2009; Yoon and Zeng 2010; Chen et al. 2013; Wu et al. 2015; Deser et al. 2017; You and Furtado 2017; Chen and Zhou 2018; Amaya 2019; Pegion et al. 2020; Zhao et al. 2020). However, the diversity of ENSO events, with different amplitudes, temporal evolutions, and spatial patterns

Supplemental information related to this paper is available at the Journals Online website: https://doi.org/10.1175/JCLI-D-21-0344.s1.

*Corresponding author*: Yingying Zhao, yzhao468@gatech.edu

DOI: 10.1175/JCLI-D-21-0344.1

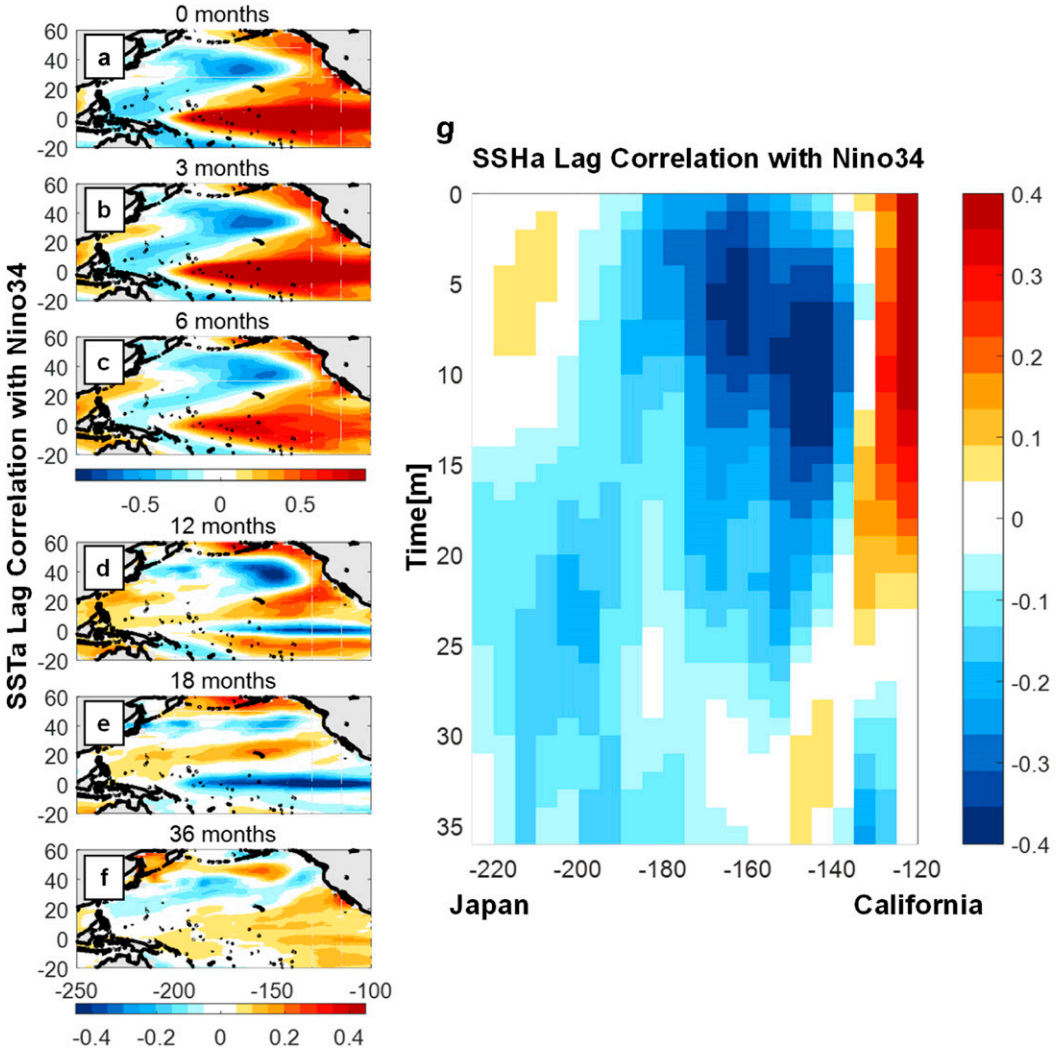


FIG. 1. (a)–(f) SSTa lag correlation maps with Niño-3.4 index for leads of 0–36 months. (g) Hovmöller diagram of SSHa lag correlation with Niño-3.4 between 28° and 45°N.

(Capotondi et al. 2015), would seem too rich to be represented by a single index or pattern at any fixed lag. For example, central Pacific ENSO events are characterized by SST anomalies centered nearer to the date line, with much weaker anomalies within the eastern Pacific cold tongue region, compared to eastern Pacific ENSO events (Kao and Yu 2009), and the leading dynamical processes driving these events are also different and may involve different time scales (Capotondi 2013; Capotondi et al. 2015, 2020b).

Even a canonical ENSO event undergoes substantial evolution over the course of its life cycle, evolving from precursor pattern through mature pattern and finally to decay pattern (e.g., Deser et al. 2010; Power et al. 2021). Some of this behavior can be seen in the series of maps in Fig. 1, which show the regression of observed SST anomalies (SSTa) against the Niño-3.4 index, at increasing lags up to 36 months. For example, starting from the mature phase of an El Niño event (lag = 0; Fig. 1a), equatorial anomalies typically display a more rapid weakening within the cold tongue region in the eastern equatorial Pacific than elsewhere, so that the center of the anomaly effectively shifts westward to the date line in the decay phase (lag = 6; Fig. 1c). Some elements of this life cycle are also reflected in decadal time scale ENSO anomalies, which are meridionally broader (e.g., continued positive correlation in the off-equatorial tropical Pacific; Fig. 1d) and have relatively larger amplitude near the date line compared to ENSO interannual patterns (Zhang et al. 1998; Power et al. 2021).

While the extratropics are particularly sensitive to Niño-3.4 SST anomalies during the peak of an ENSO event (Barsugli and Sardeshmukh 2002), extratropical teleconnections may also depend upon western tropical Pacific SST anomalies both before (Bladé et al. 2008) and after (Jong et al. 2021; Capotondi et al. 2019) the ENSO maximum. Therefore, as a method for identifying the North Pacific ENSO component, simple regression on a tropical SST index might be limited by the variety of ENSO influences on the North Pacific, which act through

both oceanic and atmospheric pathways to yield varying ENSO teleconnection patterns occurring on multiple time scales (Alexander et al. 2002 and references therein). ENSO-related equatorial Kelvin waves can propagate northward as coastally trapped waves on a time scale of a few months (Enfield and Allen 1980; Chelton and Davis 1982; Clarke and Van Gorder 1994), producing a deepening of the thermocline and warming of the coastal waveguide along the west coast of North America. This can be seen in the first few months of the Hovmöller of the lag correlation between observed sea surface height (SSH) anomalies (averaged within the 30°–45°N latitude band) and Niño-3.4, shown in Fig. 1g. Atmospheric teleconnections, in contrast, change extratropical surface winds and their corresponding surface fluxes, producing SST anomalies of opposite sign in the central and eastern North Pacific (Figs. 1a–c), These anomalies, which resemble the PDO pattern, result from integration of ENSO forcing over a period of several months, typically peaking a few months after they peak in the tropical Pacific (Fig. 1b) and continuing to persist for some time thereafter (Fig. 1c) (Alexander 1992; Alexander et al. 2002; Newman et al. 2003; Vimont 2005). In many regions of the North Pacific, these SSTa will persist 1–2 years beyond the original ENSO event due to re-emergence, or wintertime mixed layer entrainment of deeper thermal anomalies (Alexander and Deser 1995), with geographic dependence convolving both the original forcing and the local value of the mixed layer depth (Deser et al. 2003). On still longer time scales, ENSO-driven wind changes in the eastern and central North Pacific force westward-propagating oceanic Rossby waves. Initially, these are seen in the central and eastern North Pacific SSHa field within the first 10–12 months (Fig. 1g). These negative anomalies reach the Kuroshio–Oyashio Extension (KOE) region within a 2–3-yr period, consistent with the expected propagation speed of large-scale Rossby waves (Qiu 2003; Ceballos et al. 2009; Joh and Di Lorenzo 2019), where they are related to decadal fluctuations in both the ocean and atmosphere (e.g., Newman et al. 2016).

Since the physical interactions both within and between the tropical and North Pacific occur on a wide range of overlapping spatial and temporal scales, they may be better understood with a multivariate dynamical system. Here we develop such a diagnostic approach, based on empirical dynamical modeling, which allows explicit separation of the contributions of tropical and extratropical dynamics to North Pacific climate variability. Previous studies based on both observational and model data have shown that this empirical dynamical model—a linear inverse model (LIM)—is able to capture the full evolution of ENSO events and important aspects of North Pacific dynamics (e.g., Penland and Sardeshmukh 1995, hereafter PS95; Alexander et al. 2008; Newman et al. 2011, and others). Compo and Sardeshmukh (2009) used a LIM to define the tropical ENSO-related SST variations with a combination of dynamical eigenvectors of the dynamical matrix (Penland and Matrosova 2006) and then estimated the extratropical ENSO-related SST variations empirically through simultaneous regressions of the tropical ENSO-related SST. Newman (2007) constructed a LIM to study how the interactions between the tropical and North Pacific each contribute to interannual-to-decadal SST predictability, but that analysis used annual means and therefore did not capture seasonal ENSO evolution. In this work, we extend Newman's (2007) analysis by incorporating seasonal anomalies of SST and SSH in the construction of the LIM, which both captures seasonal evolution and better accounts for the ocean memory. The impact of the tropical dynamics on the North Pacific is removed in the cross-terms of the resulting linear dynamical operator to yield an "internal" North Pacific ("NP-only") dynamical system.

The long-term simulations from Earth system models (ESMs) are also powerful tools to investigate the physical mechanisms contributing to low-frequency variability of the North Pacific, and in particular to separate the remote tropical contributions from the internal extratropical dynamics. However, ESM simulations of ENSO and Pacific decadal variability appear somewhat different than observed (e.g., Newman et al. 2009; Furtado et al. 2011; Nidheesh et al. 2017; Yi et al. 2018). In particular, the interactions between the tropical and extratropical Pacific (i.e., ENSO teleconnection dynamics and ENSO precursor dynamics) on both interannual and decadal time scales are generally too weak in the ESMs (Furtado et al. 2011; Newman et al. 2016; Nidheesh et al. 2017; Zhao et al. 2021). Since the tropical–extratropical coupling has been shown to be important for the simulation of Pacific decadal variability in climate models (Newman 2007; Zhao et al. 2021), we also aim to compare the coupled tropical–North Pacific dynamics in the ESMs to what may be estimated from observations.

The paper is organized as follows. The data and approaches are explained in section 2. Section 3 compares different methods to remove tropical effects from the North Pacific. The impact of tropical dynamics on North Pacific variability in observations is examined in section 4. The role that tropical dynamics plays in the North Pacific in the climate models is discussed in section 5, where it is also compared to observations. We then conclude with a discussion and summary in section 6.

## 2. Data and methods

### a. *Observational and climate model data*

The observational data used here included monthly mean values of SST (unit: °C) and SSH (unit: m) from the European Centre for Medium-Range Weather Forecasts (ECMWF) Ocean Reanalysis System 4 (ORAS4) (Balmaseda et al. 2013) for the period January 1958–December 2015. We assessed the robustness of our results by evaluating additional SST datasets over the same period (1958–2015), including the Met Office Hadley Centre Sea Ice and Sea Surface Temperature dataset (HadISST1) dataset (Rayner et al. 2003) and National Oceanic and Atmospheric Administration (NOAA) Extended Reconstruction SST dataset, version5 (ERSST v5) (Huang et al. 2017). Monthly-mean SST and SSH output from historical simulations (r1i1p1) of 19 climate models from phase 6 of the Coupled Model Intercomparison Project (CMIP6) were also used in this study (see Table 1) (Eyring et al. 2016). The period of model data was restricted to 1950–2014.

SST and SSH fields were first averaged into 2° latitude × 5° longitude grid boxes and then smoothed in time with a 3-month

TABLE 1. List of models analyzed in the present study from the CMIP6 database. Three models (EC-Earth3, FIO-ESM-2-0, and GFDL-CM4) that have a full to NP-only LIM variance change pattern that better matches the observation are chosen as "Group 1" models. (Expansions of most acronyms are available online at http://www.ametsoc.org/PubsAcronymList).

| Model name | Class | Model name | Class |
|---|---|---|---|
| ACCESS-CM2 | | GFDL-CM4 | Group 1 |
| ACCESS-ESM1-5 | | GFDL-ESM4 | |
| BCC-CSM2-MR | | MPI-ESM-1-2-HAM | |
| CanESM5 | | MPI-ESM1-2-HR | |
| CAS-ESM2-0 | | MRI-ESM2-0 | |
| CESM2 | | NESM3 | |
| CIESM | | NorCPM1 | |
| EC-Earth3 | Group 1 | NorESM2-LM | |
| EC-Earth3-Veg | | SAM0-UNICON | |
| FIO-ESM-2-0 | Group 1 | | |

running mean. Anomalies were derived by removing the mean monthly climatology. Each field was normalized by its domain-averaged climatological standard deviation before computing the empirical orthogonal functions (EOFs) used to construct the LIM.

### b. *Using the LIM to remove tropical dynamics from North Pacific variability*

In a LIM framework (e.g., PS95), the evolution of climate anomalies is modeled as

$$\frac{d\mathbf{x}}{dt} = \mathbf{L}\mathbf{x} + \boldsymbol{\xi}, \tag{1}$$

where $\mathbf{x}$ is the anomalous climate state vector, and $\mathbf{L}$ is the linear dynamical evolution operator representing both local and non-local deterministic dynamics, which can also include linearly parameterizable nonlinear dynamics, with all remaining unpredictable nonlinear dynamics approximated as a temporally white noise forcing $\boldsymbol{\xi}$. Note that $\mathbf{L}$ can be determined based on the covariances of the state vector $\mathbf{x}$, as described in PS95

$$\mathbf{L} = \tau_0^{-1} \ln[\mathbf{C}(\tau_0)\mathbf{C}(0)^{-1}], \tag{2}$$

where $\mathbf{C}(0) = \langle \mathbf{x}(t)\mathbf{x}^{\mathrm{T}}(t)\rangle$ is the covariance matrix of $\mathbf{x}$ and $\mathbf{C}(\tau_0) = \langle \mathbf{x}(t+\tau_0)\mathbf{x}^{\mathrm{T}}(t)\rangle$ is the lag-covariance matrix at lag $\tau_0$. In this work, we chose $\tau_0 = 3$ months. Finally, the spatial statistics of the white noise forcing is determined from a fluctuation-dissipation relation:

$$\mathbf{L}\mathbf{C}(0) + \mathbf{C}(0)\mathbf{L}^{\mathrm{T}} + \mathbf{Q} = 0, \tag{3}$$

where the noise covariance matrix $\mathbf{Q} = \langle \boldsymbol{\xi}\boldsymbol{\xi}^{\mathrm{T}}\rangle dt$.

Following Newman (2007), the dynamics of the coupled system of tropical Pacific and North Pacific may be investigated by rewriting Eq. (1) as

$$\frac{d\mathbf{x}}{dt} = \frac{d}{dt}\begin{bmatrix}\mathbf{x}_T\\ \mathbf{x}_N\end{bmatrix} = \begin{bmatrix}\mathbf{L}_{TT} & \mathbf{L}_{NT}\\ \mathbf{L}_{TN} & \mathbf{L}_{NN}\end{bmatrix}\begin{bmatrix}\mathbf{x}_T\\ \mathbf{x}_N\end{bmatrix} + \begin{bmatrix}\boldsymbol{\xi}_T\\ \boldsymbol{\xi}_N\end{bmatrix}, \tag{4}$$

where $\mathbf{x}_T$ and $\mathbf{x}_N$ represent the variables within the tropical Pacific ($T$) and North Pacific ($N$), respectively. By explicitly separating the effects of $\mathbf{x}_T$ on $\mathbf{x}_N$ and vice versa, we use Eq. (4) to identify the submatrices of $\mathbf{L}$ that encapsulate internal tropical Pacific processes ($\mathbf{L}_{TT}$), internal North Pacific processes ($\mathbf{L}_{NN}$), and coupling dynamics ($\mathbf{L}_{NT}$ and $\mathbf{L}_{TN}$). The dynamics of the North Pacific in the full LIM are then

$$\frac{d\mathbf{x}_N}{dt} = \mathbf{L}_{TN}\mathbf{x}_T + \mathbf{L}_{NN}\mathbf{x}_N + \boldsymbol{\xi}_N. \tag{5}$$

We remove the effects of coupling between tropical Pacific and North Pacific by setting $\mathbf{L}_{NT} = \mathbf{L}_{TN} = 0$ in $\mathbf{L}$. Then the North Pacific system in the North Pacific–only LIM (NP-only LIM) is

$$\frac{d\mathbf{x}_N}{dt} = \mathbf{L}_{NN}\mathbf{x}_N + \boldsymbol{\xi}_N. \tag{6}$$

Finally, we solve Eq. (3) for the NP-only covariance $\mathbf{C}_{NN}(0)$, given $\mathbf{L}_{NN}$ and $\mathbf{Q}_{NN}$ [since (3) is a Sylvester's equation], and then the NP-only lag-covariance is

$$\mathbf{C}_{NN}(\tau) = \mathbf{G}_{NN}(\tau)\mathbf{C}_{NN}(0), \tag{7}$$

where $\mathbf{G}_{NN}(\tau) = \exp(\mathbf{L}_{NN}\tau)$. Note that $\mathbf{C}_{NN}(0)$ is the NP-only covariance matrix, which therefore may be used to determine NP-only EOFs.

### c. *Constructing the LIMs*

For this study, we incorporate both SST and SSH in $\mathbf{x}$, since including SSH in the LIM state vector appears to improve the representation of ocean dynamics within the LIM by including additional information of the ocean memory (e.g., Newman et al. 2011; Shin and Newman 2021). We first remove the externally forced trend from the data, since this work focuses on decoupling the unforced dynamics between tropical and North Pacific. Therefore, following the approach of Penland and Matrosova (2006) and Frankignoul et al. (2017), we estimate the externally forced trend by determining the least damped eigenmode from a LIM whose state vector $\mathbf{x}$ represents SST and SSH anomalies covering the entire Pacific basin (60°S–60°N). The time-varying projection on the least damped stationary eigenmode from this LIM (which we do not consider further) is then removed from the original data. The resulting "detrended" data form the basis for the coupled tropics–North Pacific LIM analysis, including subsequent estimation of NP-only variability. Note that we did not find these results to be qualitatively changed with different methods to remove the trend.

For this study, the (detrended) state vector $x$ comprises a tropical Pacific component $x_T$, with subcomponents $\mathrm{SST}_T$ and $\mathrm{SSH}_T$, or the SST and SSH anomalies in the tropical Pacific (14°S–14°N, 100°E–60°W), respectively; and North Pacific component $\mathbf{x}_N$, with subcomponents $\mathrm{SST}_N$ and $\mathrm{SSH}_N$, the SST and SSH anomalies in the North Pacific (20°–60°N, 100°E–60°W). The term $x$ represents the 12, 3, 12, and 2 leading PCs of $\mathrm{SST}_T$, $\mathrm{SSH}_T$, $\mathrm{SST}_N$, and $\mathrm{SSH}_N$, respectively explaining about 92%, 73%, 74%, and 27% of the variability of their respective fields. To diagnose the impact of including SSH in the LIM state vector, we also constructed an SST-only LIM, whose state vector only contains 12 (12) leading PCs of $\mathrm{SST}_T$ ($\mathrm{SST}_N$).

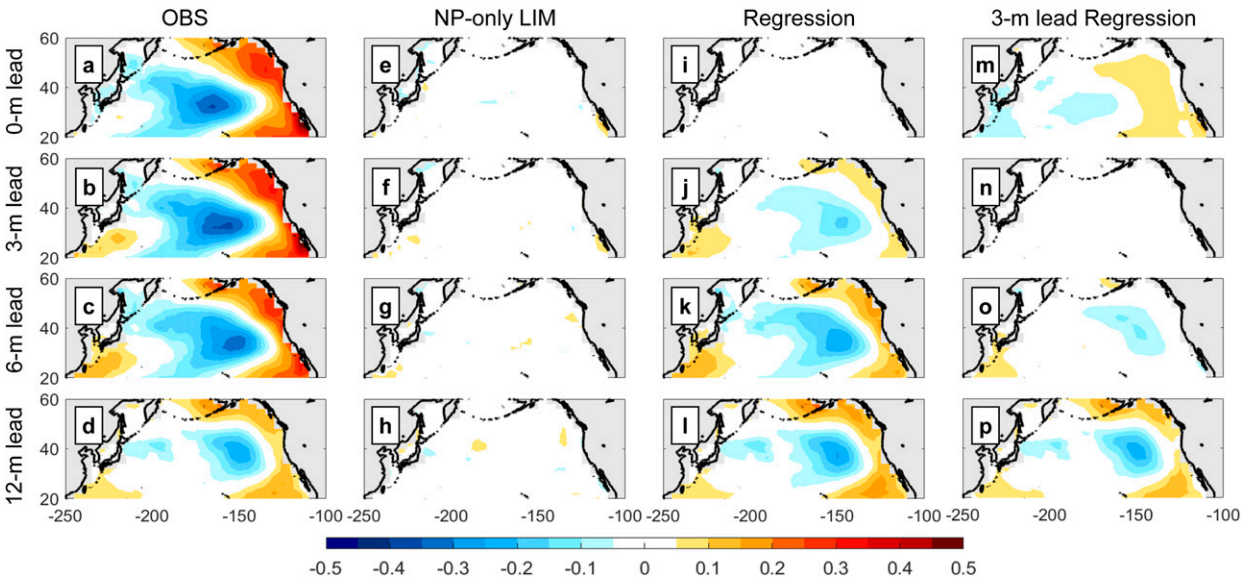


FIG. 2. North Pacific SSTa regressed on the Niño-3.4 index for leads of 0–12 months. (a)–(d) Regression maps between Niño-3.4 index and ORAS4 SSTa. The remaining columns are as in (a)–(d), except (e)–(h) for the NP-only LIM, (i)–(l) for SSTa when removing the Niño-3.4 regressed component, and (m)–(p) for the SSTa when removing the Niño-3.4 regressed component with 3-month lead.

Unfortunately, only a few SSH PCs could be retained before the LIM failed basic tests of its construction (the "Nyquist problem"; PS95; Penland 2019) that typically arise due to sampling issues (i.e., short data records). This means that the SSH variance represented by the LIM is lower than observed, although the SST variance is generally a good match (see Fig. S1 in the online supplemental material).

To use the LIM for diagnosis, we first must confirm the validity of its linear approximation. This is typically done through a tau test (PS95), where for example the LIM's (linearly) predicted lag-covariability, $\mathbf{C}(\tau) = \exp(\mathbf{L}\tau)\mathbf{C}(0) = \mathbf{G}(\tau)\mathbf{C}(0)$, is compared to the observed lag-covariability for lags greater than the training lag. Figure S1 compares the original and LIM-predicted 6- and 12-month lag-autocovariances of SST and SSH anomalies. The full LIM captures all salient aspects of the SST lag-autocovariance pattern. The LIM also generally captures SSH lag-covariance, although it underestimates amplitude at all lags, especially in the North Pacific, due to the relatively severe SSH EOF truncation (Fig. S1).

We constructed two 1000-member sets of realizations from Eqs. (4) and (6), which were then used for some analysis and significance testing in a standard Monte Carlo approach. Each equation was integrated forward for 59 000 years using the method described in Penland and Matrosova (1994), where the spatial structure of the white noise forcing $\boldsymbol{\xi}_N$ and the decoupled noise forcing $\boldsymbol{\xi}_{NN}$ was determined from the noise covariance matrices $\mathbf{Q}$ and $\mathbf{Q}_{NN}$, respectively, obtained from Eq. (3). Each resulting integration (Full LIM and NP-only LIM) was separated into 1000 ensemble members, each 59 years in length.

Although the LIMs were computed in a reduced EOF space, all comparisons to observations were done using the full (untruncated) gridded data. For the NP-only results, this means that we assumed that all residual SST and SSH variability not contained within the LIM state vector would be unchanged in the NP-only system. Since the EOF space is orthogonal, we determined this residual from

$$\mathbf{C}_g(\tau) = \mathbf{C}_{g,x}(\tau) + \mathbf{C}_{g,\text{remainder}}(\tau), \tag{8}$$

where $\mathbf{C}_g(\tau)$ is the gridded covariance of the original data, $\mathbf{C}_{g,x}(\tau)$ is the gridded covariance captured by the EOF-truncated grid space data, and $\mathbf{C}_{g,\text{remainder}}(\tau)$ is the gridded residual covariance. Note that this is true for both zero- and lag-covariance matrices, and for both the full and NP-only LIMs. In practice, the residual variability is largely noise, so the results shown below would be little changed by not including the remainder.

Finally, note that the $i$th column of the $\tau$ lag-covariance matrix $\mathbf{C}_g(\tau)$ represents the regression of $x$ against the time series of its $i$th component [e.g., $x_i(t)$] at lag $\tau$, and similarly the $i$th row represents the regression of $x$ against the time series of its $i$th component at lead $\tau$. Moreover, if we define an index as an average within some region, then the average of the columns (rows) corresponding to the grid points used to define the index gives the lead (lag) regression between $x$ and that index at lag $\tau$ (after appropriate normalization).

## 3. Comparison of different methods of removing ENSO

We start by evaluating how well the LIM isolates the tropical influence on North Pacific variability compared to methods that use regression against a single ENSO index. First, we determined the observed regression between the Niño-3.4 index and North Pacific SSTa for different lead times (Fig. 2). The simultaneous regression between the Niño-3.4 index and observed SSTa exhibits a PDO-like pattern in the North Pacific (Fig. 2a), which shifts slowly eastward and intensifies for longer lags (Figs. 2a–c), and then notably decays by about 12 months (Fig. 2d).

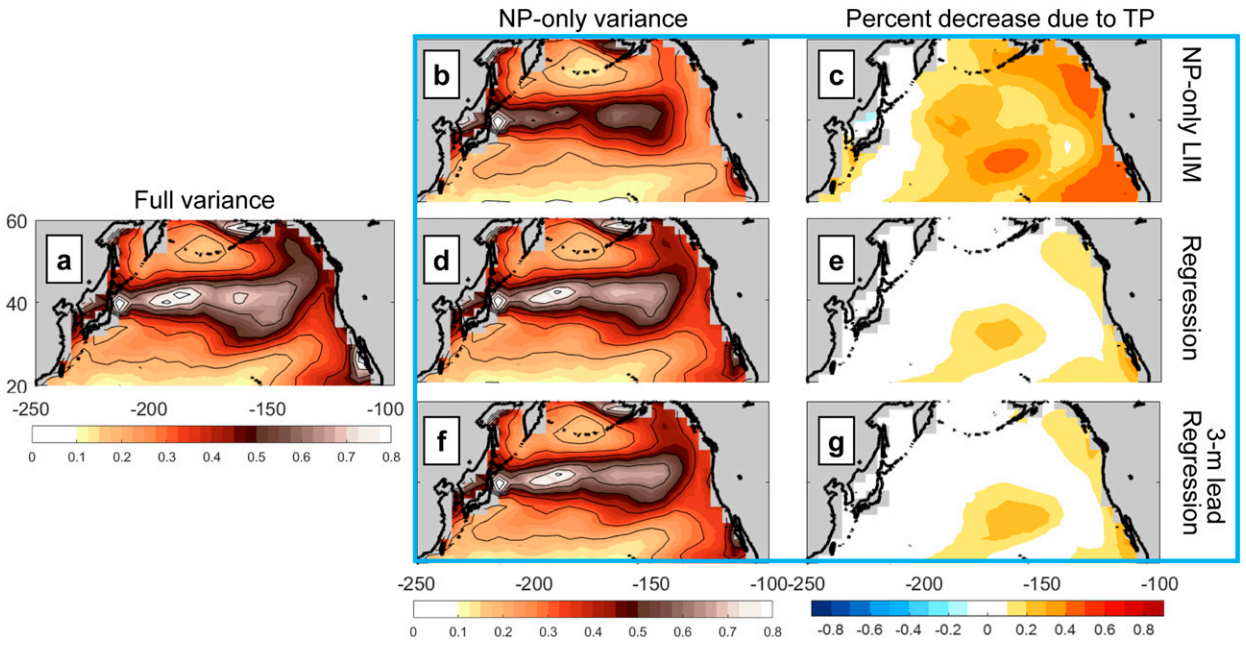


FIG. 3. ORAS4 SST variance patterns (°C$^2$) and percent changes of SST variance (%). (a) Observed full SST variance pattern. Other panels show the NP-only SST variance patterns (b) of NP-only LIM, (d) when removing Niño-3.4 regressed component, and (f) when removing the Niño-3.4 regressed component with 3-month lead; and the percent decrease from full variance to NP-only variance (c) of NP-only LIM, (e) when removing the Niño-3.4 regressed component, and (g) when removing the Niño-3.4 regressed component with 3-month lead. Removing the leading PC of the tropical Pacific regressed component will get the same results.

We next applied various methods of "removing" ENSO from the data, and then recomputed the Niño-3.4 regressions. For the NP-LIM, the remaining variability is almost uncorrelated with Niño-3.4, both simultaneously (Fig. 2e) and for all lags (Figs. 2f–h), demonstrating that all North Pacific variability both simultaneous with and subsequent to the Niño-3.4 anomaly has been successfully removed by the multivariate LIM. In the next column, we show the same calculation applied to data where only the simultaneous linear regression of Niño-3.4 index has been removed from the original data. Now, although there is no residual variability that is *simultaneously* uncorrelated with Niño-3.4, there remains a residual that has a clear relationship with Niño-3.4 for all subsequent lags (Figs. 2j–l). Matters are not improved by instead removing the 3-month lagged regression on the Niño-3.4 index, since now there are residuals correlated with Niño-3.4 in both the simultaneous (Fig. 2m) and the 6- and 12-month lead regression maps (Figs. 2o,p).

Furthermore, removing ENSO through regression on Niño-3.4 removes less North Pacific SST variance (Figs. 3d–f) than the LIM method (Fig. 3b), especially near 40°N and along the coast of North America. As a result, the percent decrease from the full SST variance (Fig. 3a) to NP-only variance (Figs. 3b,d,f) due to the tropical influence is much smaller when using the regression method (Figs. 3e,g) than when using the LIM method (Fig. 3c).

Perhaps the issue is that Niño-3.4 is not the best index to represent ENSO's influence on the North Pacific. Following Takahashi et al. (2011), two different ENSO indices E = (PC1 + PC2) and C = (PC1 − PC2) were constructed, where PC1 and PC2 are the first and second leading PC of tropical Pacific SSTa, respectively. These indices are sometimes considered to represent eastern Pacific (E) and central Pacific (C) ENSO types (e.g., Capotondi et al. 2015). Similar to the analysis using the Niño-3.4 index, we removed the simultaneous linear regression of either E (Figs. 4a–e) or C (Figs. 4f–j) from the original data. In agreement with Chen and Wallace (2016), we found that removing the regression against C had almost no impact on North Pacific SSTa, while the regression against E had a somewhat greater impact on North Pacific SSTa than the Niño-3.4 regression. However, its impact was still much smaller than that obtained from the NP-only LIM (Fig. 3c). Moreover, after removing the regressed components, the lagged relationship between either C or E and North Pacific SSTa still remained, with considerable amplitude especially at longer leads (Figs. 4d,e,i,j). That is, removing the linearly regressed component against a single ENSO index, either simultaneously or at a fixed lag, from North Pacific SSTa is unable to fully remove the variance associated with the spatial–temporal evolution of tropical ENSO dynamics, and substantially underestimates the influence of ENSO upon the North Pacific. Decoupling the North Pacific from the entire tropical Pacific through the LIM method more definitively removes the tropical impact on North Pacific variability.

## 4. Impact of tropical dynamics on observed North Pacific variability

### *a. Overall variability*

To evaluate the overall impact of tropical dynamics upon North Pacific variability, we first compare the SST variance

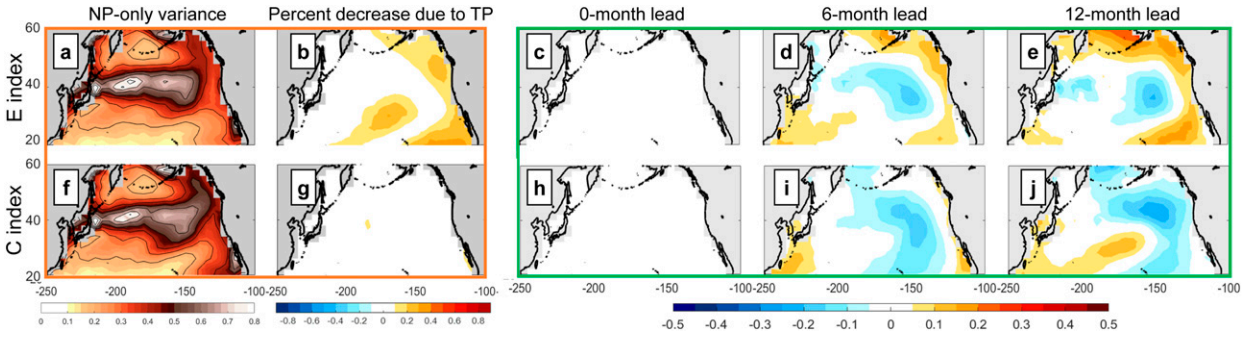


FIG. 4. SST variance patterns ($°C^2$) and lead–lag regression maps. (a) NP-only SST variance pattern. (b) Percent decrease due to tropical Pacific when removing linear regression of E index (PC1 + PC2). PC1 and PC2 are the first two leading PCs of the tropical Pacific. (c)–(e) Regression maps between E index and SSTa when removing linear regression of E index. (f) Internal SST variance pattern. (g) Percent decrease due to tropical Pacific when removing linear regression of C index (PC1 − PC2). (h)–(j) Regression maps between C index and SSTa when removing linear regression of C index.

pattern of the full and NP-only LIM in the observational analysis (Figs. 3a–c; see also Fig. S2 for dataset sensitivity of the observational results). The full SST variance has high amplitude in the KOE region and the two main centers of the PDO pattern, north of Hawaii and along the coast of North America (Fig. 3a). In contrast, after removing the tropical influence, the NP-only variance (Fig. 3b) is substantially reduced; notably, variance is almost halved in the terminus of the atmospheric bridge, along the coast of North America, and within the Subtropical Front (around 30°N near Hawaii) (Fig. 3c). On the other hand, the variance within the KOE region (around 40°N) and along the coast of East Asia is little changed. Tropical forcing also contributes about 20% of the SSH variance to the maximum within the KOE region and more broadly throughout much of the North Pacific (cf. Figs. S3a–c). In conclusion, tropical dynamics have an important impact on SST and SSH variance in the North Pacific, especially along the North American coast and in the subtropical area around 30°N in observations (Fig. 3c; see also Fig. S3c).

### b. *Climate modes*

We next explore how tropical dynamics drive patterns of variability in different regions of the North Pacific. First, we define a KOE index as the average SSH anomaly in the region bounded by 31°–36°N and 140°–165°E, and a central North Pacific (NP) SST index as the average SST anomaly in the region bounded by 30°–38°N and 170°–155°W. These are used to determine lead–lag regressions from $\mathbf{C}_{g,\text{NP-only}}(\tau)$ (see section 2). The lead–lag regression maps between the KOE index and the SSTa/SSHa fields show that the observed SSTa evolution associated with the KOE index (left column of Fig. 5) is little changed and only somewhat weakened in the NP-only system (right column of Fig. 5), suggesting that both the amplitude and evolution of KOE SSTa/SSHa variations are primarily driven by internal North Pacific dynamics.

The lead–lag regression maps based upon the central NP SST index capture the evolution of a PDO-like pattern (Fig. 6). Here, the removal of the tropical forcing leads to substantial change, notably the reduction of both the horizontal scale and amplitude of the SST and SSH central North Pacific maxima in the NP-only regression compared to the observed regression, as well as the virtual elimination of the anomaly along the North American coast associated with ENSO teleconnections (cf. Figs. 6c and 6h). Additionally, Fig. 6 shows that the central Pacific anomaly in the NP-only system is short-lived (right column), with a time scale of only a few months, especially compared to the considerably more persistent anomaly seen in observations (left column). Note that similar results are obtained using other observational datasets instead (ERSST v5 and HadISST), shown in Fig. S4. These results suggest that, while Aleutian low variations can be driven both internally and through ENSO teleconnections, their effect on central North Pacific SSTa/SSHa variability may be quite different, with more persistent ENSO forcing driving a larger-scale, more persistent response than is obtained from rapidly decorrelating weather forcing.

Given this picture of NP-only variability, we next ask how the dominant patterns of North Pacific SSTa and SSHa would be different in the absence of tropical forcing; for example, would the leading EOF of observed SSTa still resemble the PDO without tropical forcing? To answer this question, in Fig. 7 we compare the leading North Pacific SSTa and SSHa EOFs determined from $\mathbf{C}_{g,\text{NP-only}}(0)$, the zero-lag covariance matrix determined for the NP-only system, to the leading EOFs determined from the original data, where the SSTa EOFs are indicated by shading and the SSHa EOFs by contours. In observations, the leading North Pacific SSTa EOF (Fig. 7a) is the well-known PDO dipole pattern, with a central Pacific maximum tilted west-northwest from north of Hawaii to Japan and an opposite-polarity anomaly of roughly equal amplitude curving along the eastern boundary. In contrast, the leading NP-only SSTa EOF (Fig. 7b) is largely monopolar, zonally aligned along the subarctic front and extending eastward from Japan (along 40°N) to a maximum located somewhat northward of the original PDO maximum. Such a pattern has been associated with SSTa variability driven by changes in the strength and position of the Oyashio (e.g., Frankignoul et al. 2011), and we will refer to it as the KOE pattern hereafter. This change of the dominant SSTa mode of variability after decoupling from the tropical Pacific, from a PDO-like to a

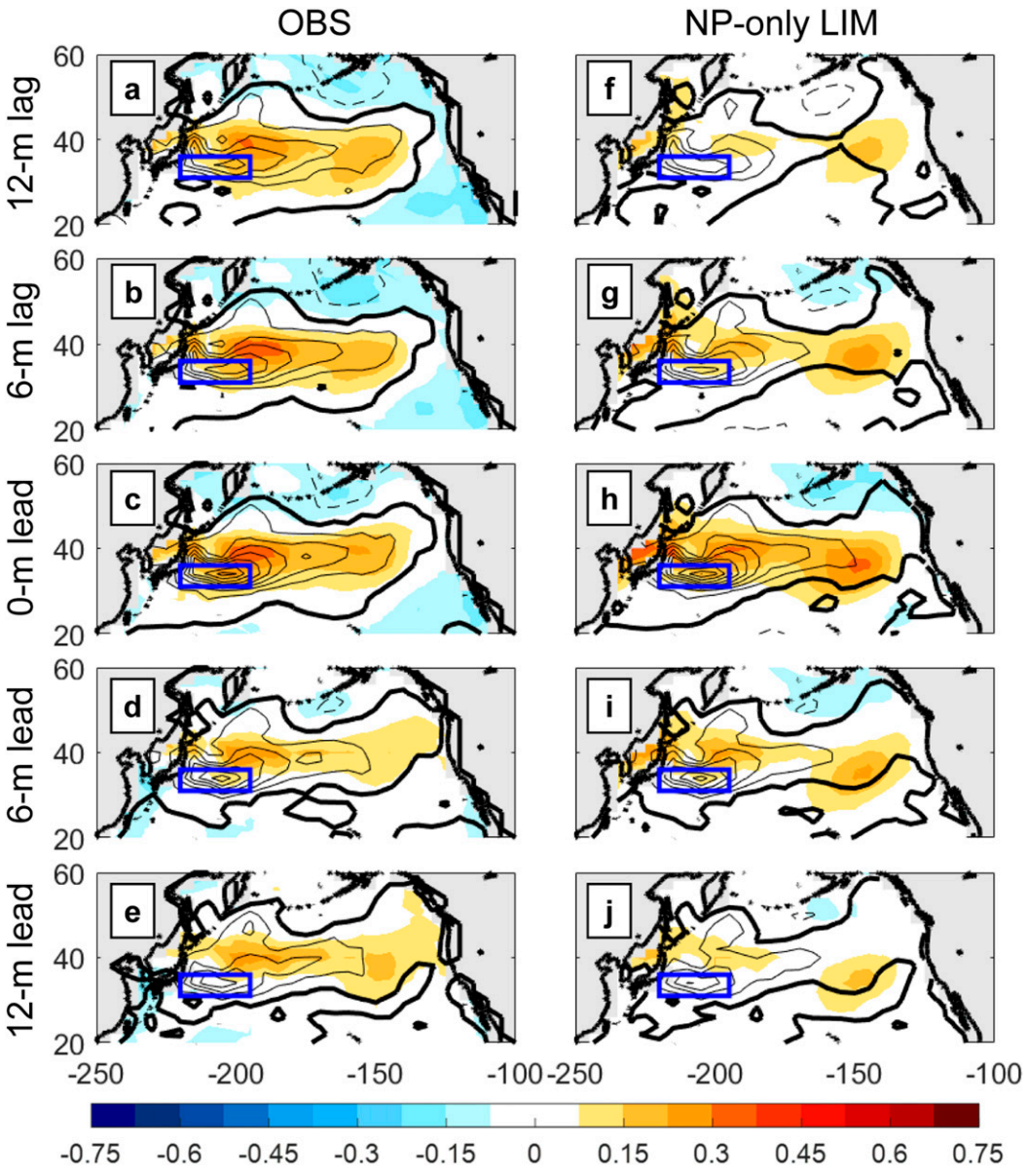


FIG. 5. Lead–lag regression maps between the KOE index and SSTa/SSHa field. (a)–(e) Lead–lag regression maps between KOE index and SSTa(shading)/SSHa(contours) of ORAS4. (f)–(j) As in (a)–(e), but for the NP-only system. The contour interval of SSHa is 0.0075.

KOE-like pattern, also results when repeating our analysis using other observational datasets (Fig. S5) and is consistent with the change of overall SST variance discussed above.

The leading SSH EOF (contours in Figs. 7a,b) is also influenced by the tropical forcing, with a KOE-like pattern that is much more localized to the western Pacific in the NP-only LIM (Fig. 7b), instead of the basinwide PDO-like pattern in observations (Fig. 7a).

Autocorrelation functions of the PCs corresponding to these EOFs were also determined, to study the tropical impact on the persistence of these dominant modes of variability (Fig. 7c; see also Figs. S5e,f and S6). In the NP-only LIM, the autocorrelation function of a selected PC can be obtained by projecting the NP-only spatial covariance matrices $\mathbf{C}_{g,\text{NP-only}}(\tau)$ onto the corresponding EOF pattern. Decoupling from the tropical Pacific reduces by half the time scale of both the North Pacific dominant SST mode (Fig. 7c; see also Figs. S5e,f) and the dominant SSH mode (Fig. S6a), compared to observations.

### c. *Low-frequency variability*

The results of the previous section suggest that tropical forcing drives NP variability not only to be stronger, especially in the eastern part of the basin, but also to be more persistent. This raises the possibility that the tropics could likewise have

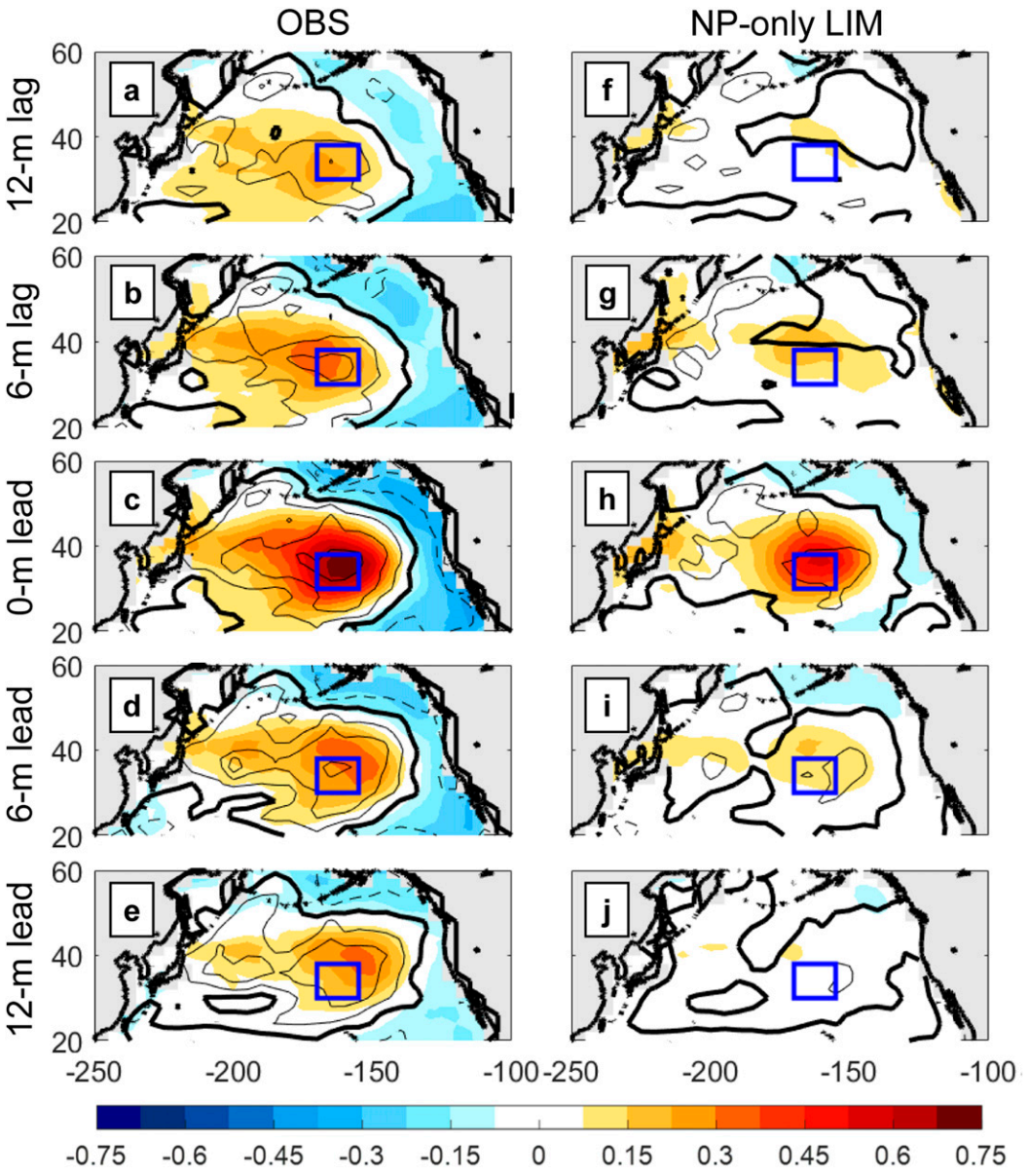


FIG. 6. Lead–lag regression maps between central NP SST index and SSTa/SSHa field. (a)–(e) Lead–lag regression maps between central NP SST index and SSTa(shading)/SSHa(contours) in ORAS4. (f)–(j) As in (a)–(e), but for the NP-only LIM system. The contour interval of SSHa is 0.0075.

an impact on North Pacific low-frequency climate variability. Therefore, in this section, we repeat our analysis, but first filter out higher frequencies including those associated with ENSO interannual variability. To do this, we apply the Zhang et al. (1997) low-pass filter, which acts to remove power associated with periods less than 6 years, to SSTa and SSHa from both observations and the LIM ensemble data.

The impact of tropical dynamics on North Pacific SST anomalies is even more pronounced for low-frequency variability, with the notable exception of the KOE region. Observed low-pass SST variance, shown in Fig. 8a, has a pattern quite similar to the total SST variance (Fig. 3a), including KOE-like and PDO-like variability. In the central North Pacific and the coastal region of North America, where the influence of ENSO teleconnections is strongest, the low-pass variance represents a somewhat larger fraction (~30%) of the total variance than elsewhere (Fig. 8b). In comparison to these observations, NP-only low-pass variance (Fig. 8c) is sharply reduced in most regions of the North Pacific, especially along the coast of North America and in the Subtropical Front (Fig. 8d). In the KOE region, however, the NP-only and total low-pass variance are largely the same.

Involving SSH in the LIM tends to improve its representation of observed SST variability on longer time scales. The

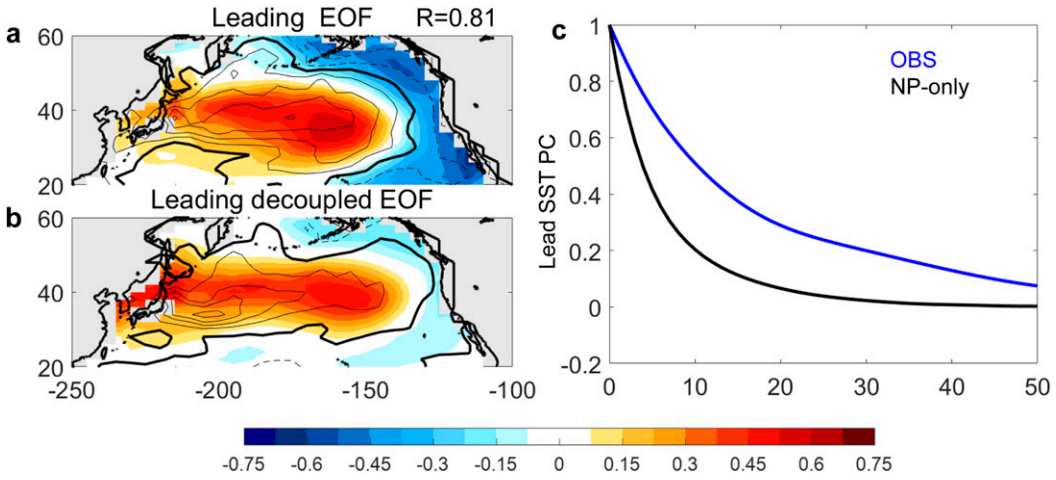


FIG. 7. Dominant patterns of the North Pacific and autocorrelations of the dominant SST PCs of the North Pacific. Leading EOF pattern of the North Pacific of (a) ORAS4 and (b) NP-only LIM. The shading shows the SST patterns, and the contours show the corresponding SSH patterns. The SSH contour interval is 0.01. (c) Observational autocorrelation function of the leading SST PC of North Pacific (blue line) and autocorrelation function calculated from spatial covariance matrix of the NP-only LIM (black line).

SST-only LIM performed slightly worse than the SST–SSH LIM, with an underestimation of observed SST lag-covariance especially at longer time scales (18–24 months) (Fig. S7). Consequently, the NP-only version of the SST-LIM was also less persistent (Fig. S7) and the relative impact of the tropics on North Pacific SST variability was only slightly stronger, both overall (Fig. S8) and on decadal time scales (Fig. S9).

## 5. Comparison between observations and CMIP6

ESMs are another powerful tool to understand how the physical mechanisms contribute to the low-frequency variability of the North Pacific. Therefore, in this section we evaluate 19 climate models from CMIP6, to understand how well they are able to capture observed North Pacific variability and its interactions with the tropics. First, updating the Newman et al. (2016) analysis of the CMIP3/-5 models, we compare the dominant EOF pattern of North Pacific variability in each CMIP6 model to observations. Figure 9a shows this comparison in the form of a Taylor diagram, where each model EOF is compared to the observed (ORAS4) EOF (i.e., the PDO). The leading SST EOF patterns from the other SST datasets are also compared to the ORAS4 EOF (Fig. 9a, black and blue pentagrams), showing that they are fairly similar across the three SST datasets we examined. In contrast, the CMIP6 models (diamonds in Fig. 9a) all have much poorer matches to the observed EOF, well outside the range of observational uncertainty. Moreover, the model EOFs appear significantly outside the range expected by sampling. This is shown by the gray dots in Fig. 9, which indicate the comparison of each leading EOF determined from each of 1000 different LIM 59-yr realizations to the observed EOF (see section 2 for more details). The CMIP6 EOFs are more different from the observed EOF than over 90% of the LIM realizations (Fig. 9a, dark gray dots), implying that the differences between the leading observed and model North Pacific SST EOFs are statistically significant and likely due to model error rather than the limitation of a single observational realization. This is even true for the dominant North Pacific SST EOF computed from the CMIP6 multimodel ensemble mean (MEM; orange pentagram) covariance matrix.

We next built LIMs from the output of each model and repeated the observational LIM analysis. The multimodel ensemble mean statistics are determined by the arithmetic mean of the statistics analyzed in each model. For example, the full SST variance pattern of each model is first obtained, and then full SST variance patterns of all models are averaged collectively as the MEM full SST variance pattern.

The MEM of the North Pacific SST variance shows very strong variability, especially within the KOE region (Fig. 10a), yet is absolutely weaker along the North American coast and relatively weaker within the central North Pacific compared to observations (Fig. 3a). Moreover, compared to the full SST variance in the MEM, the NP-only variance is relatively little changed (cf. Figs. 10a and 10b), with a reduction of only about 10%–20% (Fig. 10c). This suggests that North Pacific SST variability is considerably less influenced by tropical dynamics in the CMIP6 models than in observations (Fig. 3c). Similarly, the excessive SSH variability within the KOE region in the MEM remains nearly unchanged in the NP-only LIM (Figs. S3d–f), again in sharp contrast to the observational analysis (Figs. S3a–c) and again implying that the contribution of the tropical dynamics to SSH variability is too small in the CMIP6 models. These results suggest that while tropical dynamics play an important role in shaping the variability of the North Pacific in the observations, ESMs are far less sensitive to tropical forcing, so that their North Pacific variability—which appears too strong—is primarily reflective of internal extratropical processes.

Given these results, it is not entirely unexpected that the dominant North Pacific SST EOF for the MEM has

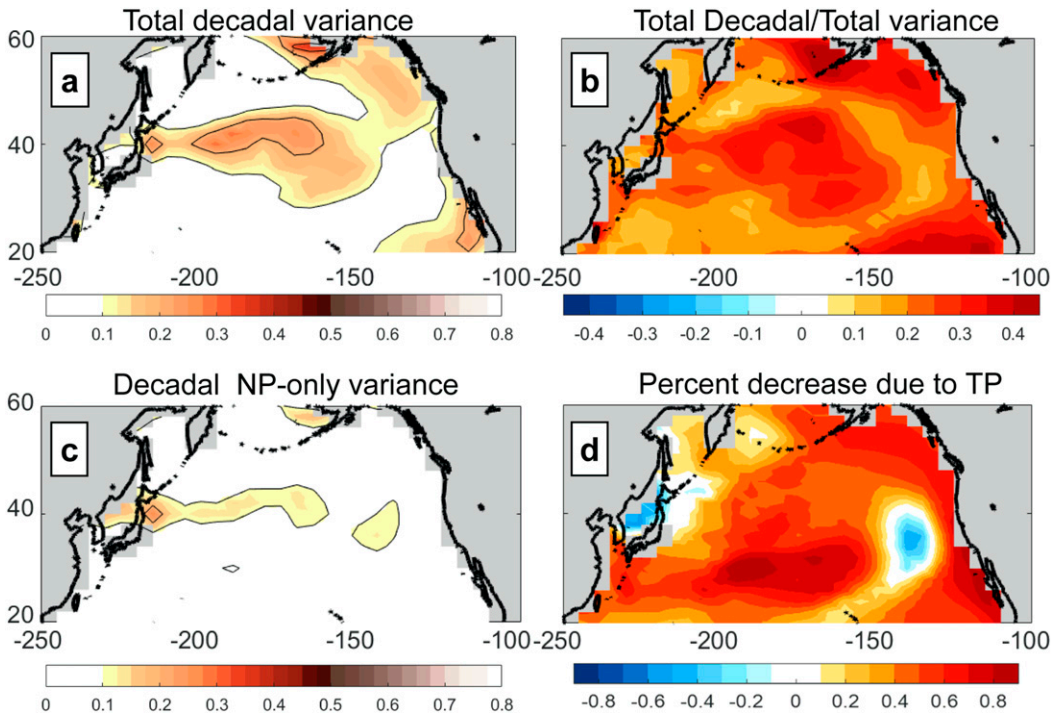


FIG. 8. (a) Total decadal SST variance pattern ($°C^2$) when applying a 6-yr low-pass filter onto the SSTa field. (b) The ratio of decadal variance to total variance. (c) Decadal NP-only variance pattern when applying a 6-yr low-pass filter onto NP-only LIM integrated SSTa field. (d) Percent decrease from total decadal variance to internal decadal variance.

characteristics more similar to the KOE pattern (Fig. 11a) than to the observed PDO (Fig. 7a). Removing the tropical influence from the North Pacific does not notably change this pattern (Fig. 11b), with a spatial correlation coefficient of 0.97 between the original and NP-only EOF pattern, again consistent with a model underestimation of the tropical–North Pacific relationship, also consistent with previous findings (e.g., Furtado et al. 2011; Nidheesh et al. 2017; Zhao et al. 2021).

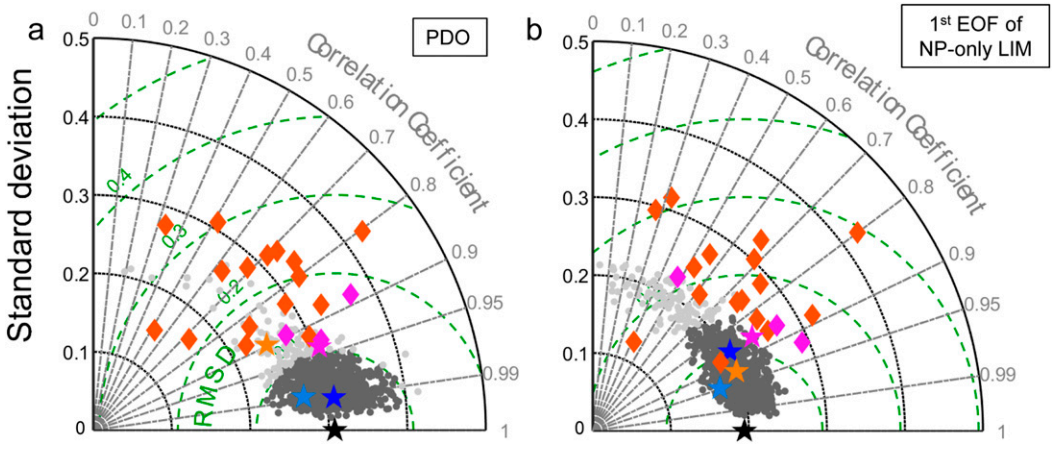


FIG. 9. Taylor diagrams of (a) leading EOF pattern of North Pacific SSTa (PDO), (b) leading EOF pattern of North Pacific SSTa of NP-only LIM. Black star: ORAS4. Blue star: ERASST. Light blue star: HadISST. Orange star: MEM. Magenta star: Group1 MEM. Magenta diagrams: Group 1 models. Red diamonds: other CMIP6 models. Gray dots show the estimates based on the 59-yr Monte Carlo subsamples, in which the dark gray dots show the 90% confidence level of these patterns using the 1000 samples and the light gray dots show the other patterns. In a Taylor diagram, the distance of a point from the reference point (black pentagram, ORAS4) indicates the level of similarity between the corresponding model and the observation.

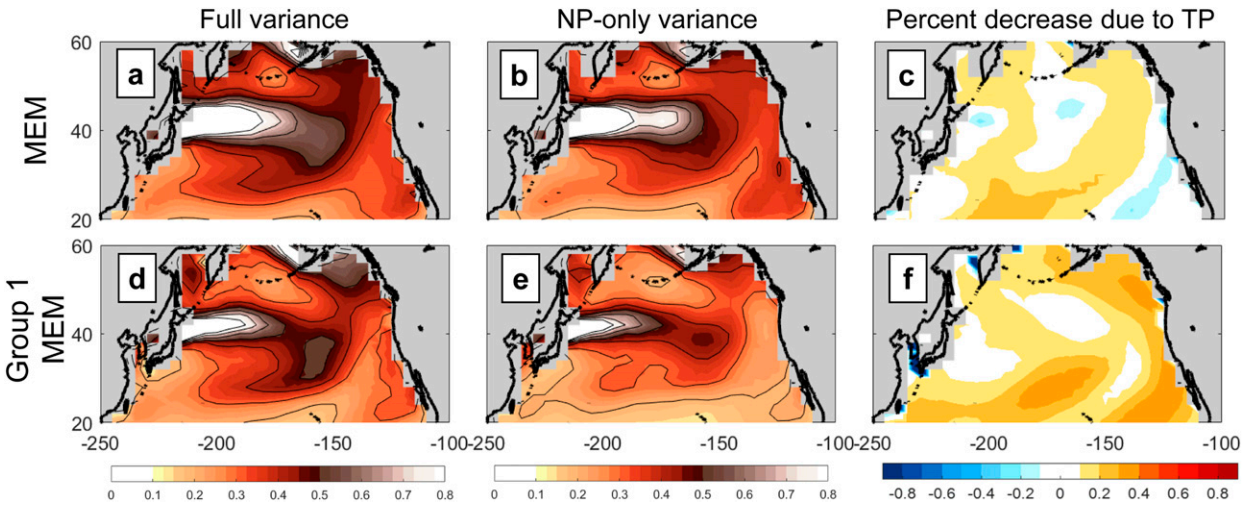


FIG. 10. MEM SST variance patterns ($°C^2$) and percent changes of SST variance from full LIM to NP-only LIM. Shown are full SST variance patterns of (a) CMIP6 MEM and (d) Group 1 MEM, NP-only SST variance patterns obtaining form NP-only LIM of (b) CMIP6 MEM and (e) Group 1 MEM, and percent changes from full variance to NP-only variance of (c) CMIP6 MEM and (f) Group 1 MEM.

Moreover, the leading North Pacific SST EOFs from all the NP-only model LIMs are considerably different than the observed, and again more different than that obtained from the 1000 LIM realizations (Fig. 9b). A comparison of the autocorrelation functions of the leading North Pacific SST PCs in the full and NP-only systems shows that while tropical forcing lengthens the time scale of the dominant NP SST mode (Fig. 7c; see also Figs. S5e,f) and SSH mode (Fig. S6a), leading to stronger low-frequency variance in observations, it does not in the CMIP6 models (Fig. 11e and Fig. S6b).

The evolution of the KOE index regression is little impacted by the tropics (cf. first and second columns of Fig. 12), even less than the small observed impact (cf. Fig. 5), again implying that the KOE-related pattern is largely driven by internal North Pacific dynamics in the ESMs. However, unlike observations, the tropics do not appear to impact the development of the central Pacific anomaly (cf. third and fourth columns of Fig. 12), whose strength and persistence lies between the observed NP-only and full systems (cf. Fig. 6). This raises the possibility that compared to observations, MEM PDO-like variability may be both too sensitive to internal North Pacific dynamics (e.g., forcing by the Aleutian low) and not sensitive enough to the tropics.

None of the CMIP6 models captures the observed pattern of the change of North Pacific SST variance due to decoupling from the tropics (cf. Fig. 3c and Fig. S10), again suggesting that they do not correctly simulate the impact of the tropical dynamics on the North Pacific. Still, a few models appear to better match observations than even the MEM, so perhaps they better capture observed dynamics as well. We explore this possibility by selecting three models (EC-Earth3, FIO-ESM-2-0, and GFDL-CM4) whose patterns of full to NP-only variance change better match the observed. These three ''Group 1'' models (magenta diamonds in Fig. 9) also better simulate the observed PDO pattern (magenta diamonds in Fig. 9a) and exhibit more variance along the North American coast and in the central North Pacific, although as in the other models they still appear to overestimate KOE variability (Fig. 10d). The impact of tropical dynamics on the NP SST variance in a MEM derived just from the Group 1 models (Fig. 10f) is considerably more similar to observations (Fig. 3c), with a spatial correlation coefficient higher than 0.4 (magenta pentagram in Fig. S10). However, Group 1 otherwise showed no obvious improvement relative to the other models, either in terms of the dominant EOF of the NP-only variability (Figs. 11 and 9b) or in terms of the tropical impact on the evolution of the KOE and central NP regression patterns (not shown). Other methods to group the models did not yield better comparisons to observations, although averaging models tends to reduce the individual biases. Therefore, the inability to adequately capture the tropical Pacific dynamical impact on North Pacific variability appears common to all CMIP6 models, a problem that appears to have persisted at least since CMIP3/-5 (e.g., Solomon et al. 2011; Newman et al. 2016).

## 6. Concluding remarks

We quantified the role of the tropical–extratropical coupled dynamics in energizing North Pacific climate variability, using an empirical dynamical model (LIM) that allowed us to selectively and objectively include or exclude the tropical coupling, following Newman (2007). We found that tropical dynamics drive a large fraction of the central and eastern North Pacific footprint of the PDO pattern (Figs. 3 and 6). The internal variability of the North Pacific is most pronounced within the KOE region, and specifically along the subarctic front (Fig. 3), especially on decadal time scales (Fig. 8). Therefore, in the absence of tropical forcing, the dominant pattern of North Pacific variability might be characterized by a KOE-like pattern, rather than the PDO (Fig. 7). The tropical dynamics also contribute to the persistence of North Pacific anomalies (Fig. 7; see also Figs. S7 and S8) and therefore to an

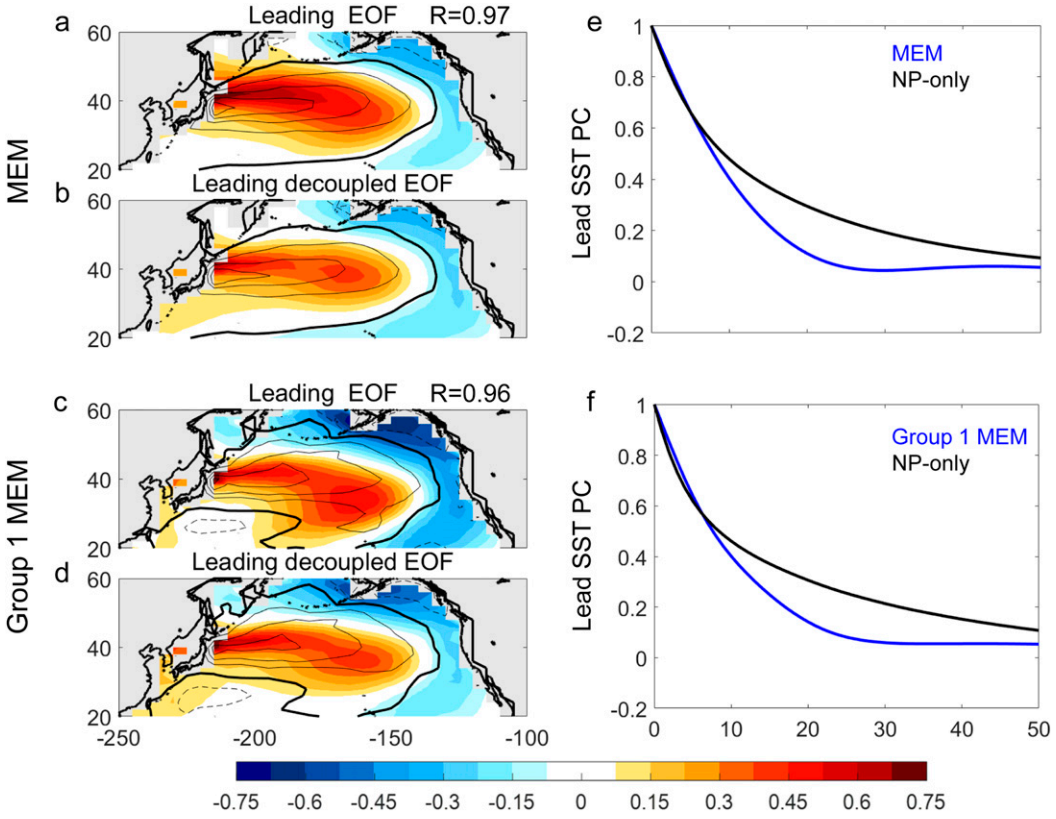


FIG. 11. As in Fig. 7, but for (a),(b),(e) CMIP6 MEM and (c),(d),(f) Group1 MEM.

even greater fraction of the low-frequency variance in the North Pacific region (Figs. 8).

Our analysis suggests that the impact of the tropics on North Pacific SST variability has been underestimated by many previous regression-based studies, as shown in Figs. 3 and 4, due perhaps to an inadequate prior definition of ENSO and an inadequate prior expectation of ENSO impacts on the North Pacific. Neither of these would necessarily be problematic if all important physical interactions within the coupled tropical–North Pacific system could be represented by a set of physically based orthogonal modes. That is, if the leading EOFs (or some suitable orthogonal rotation) of tropical and North Pacific SSTa corresponded to true physical modes of the system, such that each EOF pattern represented one distinct physical mechanism and time scale (e.g., Monahan et al. 2009), then a simple regression on the appropriate ENSO index should remove all the tropical–North Pacific dynamics associated with that index on *all* time scales. The failure of the regression method to do this—in particular, the substantial residuals remaining in the lag regression in Figs. 2j–l, 4d,e, and 4i,j—strongly supports an alternative view, previously suggested for ENSO (PS95; Capotondi et al. 2015) and the PDO (Newman et al. 2016) in the ocean, and the Pacific–North American (PNA; Henderson et al. 2020) and the North Atlantic Oscillation (NAO; Albers and Newman 2021) patterns in the atmosphere: a single pattern of variability does not correspond to a single dynamical mode, but rather arises through the combination of a number of different dynamical modes, where each mode may have a similar spatial pattern but evolve quite differently due to different underlying physical processes (i.e., they are nonorthogonal). Then, a diagnosis of the "impact" of this pattern of variability would, at a minimum, require separate removal of the effects of each of these physical modes. In essence, this is what the LIM does.

Our analysis also shows that, both individually and in the aggregate, CMIP6 models considerably underestimate the tropical influence on North Pacific variability. At the same time, they capture KOE variability that is generally similar to (although perhaps considerably stronger than) what is observed. Therefore, perhaps because of the weaker coupling with the tropics, the dominant pattern of North Pacific SST variability in most of the models is the KOE pattern. That is, the models do not in fact appear to reproduce the observed PDO (Fig. 9a), an issue that has existed for many model generations. For example, Newman et al. (2016) showed similar issues with the leading North Pacific SSTa EOF in CMIP5 models, and also found that the PDO connections to the tropics were generally too weak compared to observations, perhaps due in part to ENSO simulation errors (e.g., Bellenger et al. 2014; Capotondi et al. 2015), including the long-standing westward shift of the modeled ENSO pattern (e.g., Joseph and Nigam 2006) that results in downstream errors in ENSO teleconnections (e.g., Deser et al. 2018). As a result, diagnostic studies of North Pacific variability using CMIP-class models may routinely overestimate the importance of internal North

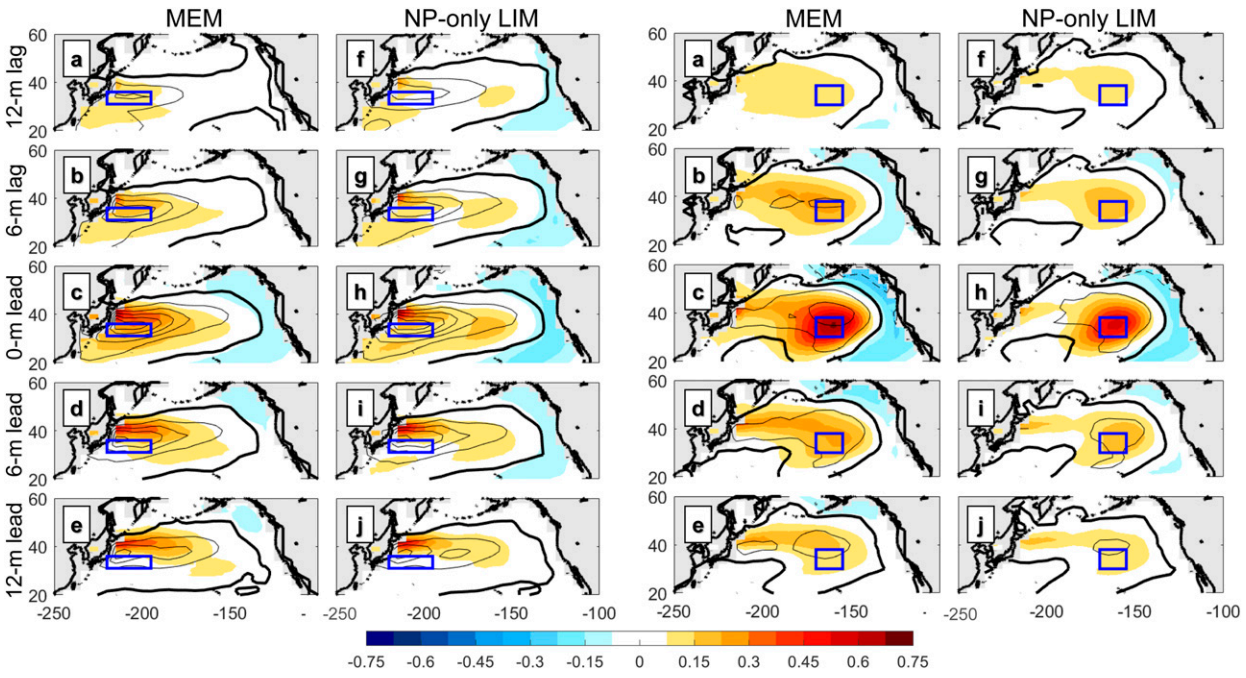


FIG. 12. As in Figs. 5 and 6, but for CMIP6 MEM. The SSHa contour interval is 0.0075.

Pacific dynamics and underestimate the importance of tropical interactions, and should be treated with considerable caution. In the meantime, diagnostic studies to determine the sources for this vexing error in the models seem to be needed.

An alternative approach to our empirical analysis is to design different numerical sensitivity experiments within climate models that aim to isolate ENSO-induced variability (e.g., Liu et al. 2002; Wang et al. 2012; Sandeep et al. 2014; Niranjan Kumar et al. 2016; Zhang et al. 2018). For example, Pacific Ocean–Global Atmosphere (POGA) experiments, in which anomalous SST over the tropical Pacific is restored to observations but elsewhere is coupled to the atmosphere (e.g., Zhang et al. 2018), have found that tropical Pacific-forced and internal components are distinct for both the PDO and South Pacific decadal oscillation. By performing a set of experiments similar to the POGA in coupled ocean–atmosphere models, Liu et al. (2002) suggest that decadal variability in the North Pacific originates predominantly from local dynamical processes; Wang et al. (2012) find the PDO variability only increases slightly in the ENSO run compared with the no-ENSO run. However, given our result that climate models do not appear to simulate observed ENSO teleconnection dynamics with complete fidelity, there may be some questions about the ability of such model experiments to entirely diagnose the tropical dynamical impact upon observed decadal North Pacific variability.

The results from the analyses presented in this paper do not imply that all of North Pacific variability is "forced" by the tropics, since tropical variability itself can be influenced by the North Pacific (Penland and Sardeshmukh 1995; Moore and Kleeman 1996; McPhaden and Yu 1999; Rodríguez-Fonseca et al. 2009; Kucharski et al. 2016; Liu and Di Lorenzo 2018; Liguori and Di Lorenzo 2019; Chung et al. 2019; Zhao and Di Lorenzo 2020). For example, some of the tropical Pacific decadal variability that drives the North Pacific is impacted by the North Pacific ENSO precursor dynamics (Zhao and Di Lorenzo 2020; Zhao et al. 2021). Removing tropical dynamics from the North Pacific using the LIM also reduces the decadal variance that is generated from extratropical ENSO precursor dynamics and then amplified by the tropical dynamics. In this work, the decoupled LIM provides a quantitative measure of the net role of tropical–extratropical coupling on North Pacific climate variability, which includes ENSO teleconnections both to and from the tropics.

To follow up on this study, we could expand upon the datasets used here, such as by extending the time range, using additional reanalysis datasets (e.g., CERA-20C; Patrick et al. 2018), and/or incorporating ocean variables that might better capture ocean dynamics than SSH. Extending the data record, either by analyzing other datasets or by using long centennial-scale climate model simulations, might also allow for consideration of nonstationarity in both ENSO dynamics (e.g., Capotondi and Sardeshmukh 2017) and the interactions between the tropics and North Pacific. We could also construct a LIM that includes surface atmospheric variables, such as mean sea level pressure and/or heat and momentum fluxes, to diagnose the dynamical role of the atmospheric bridge in coupling the tropical and North Pacific basins. Finally, the approach outlined in this study could be useful to revisit the coupling dynamics between the tropical Pacific and other oceanic regions such as the South Pacific.

*Acknowledgments.* There are no conflicts of interest for any author. This work is funded by the U.S. Department of Energy under Grant 350660B. AC was supported by the NOAA

Climate Program Office's Climate Variability and Predictability (CVP) and Modeling Analysis Predictions and Projections (MAPP) programs. MN thanks Y.-O. Kwon, C. Frankignoul, and M. Alexander for conversations that spurred early development of this analysis. The authors acknowledge the Working Group of World Climate Research Programme (WCRP) on CMIP6 Coupled Modeling, as well as the Program for Climate Model Diagnosis and Intercomparison (PCMDI) for collecting and archiving the CMIP6 model output. We thank the various climate-modeling groups for producing and making their simulations available for analysis.

*Data availability statement.* The CMIP6 data were obtained from https://esgf-node.llnl.gov/projects/cmip6/. The ORAS4 output was obtained from http://icdc.cen.uni-hamburg.de/projekte/easy-init/easy-init-ocean.html. Other observational SST data were obtained from https://psl.noaa.gov/data/gridded/data.noaa.ersst.v5.html (ERSSTv5) and https://www.metoffice.gov.uk/hadobs/hadisst/data/download.html (HadISST).

## REFERENCES

Albers, J. R., and M. Newman, 2021: Subseasonal predictability of the North Atlantic Oscillation. *Environ. Res. Lett.*, **16**, 044024, https://doi.org/10.1088/1748-9326/abe781.

Alexander, M. A., 1992: Midlatitude atmosphere–ocean interaction during El Niño. Part I: The North Pacific Ocean. *J. Climate*, **5**, 944–958, https://doi.org/10.1175/1520-0442(1992)005<0944:MAIDEN>2.0.CO;2.

——, and C. Deser, 1995: A mechanism for the recurrence of wintertime midlatitude SST anomalies. *J. Phys. Oceanogr.*, **25**, 122–137, https://doi.org/10.1175/1520-0485(1995)025<0122:AMFTRO>2.0.CO;2.

——, I. Bladé, M. Newman, J. R. Lanzante, N.-C. Lau, and J. D. Scott, 2002: The atmospheric bridge: The influence of ENSO teleconnections on air–sea interaction over the global oceans. *J. Climate*, **15**, 2205–2231, https://doi.org/10.1175/1520-0442(2002)015<2205:TABTIO>2.0.CO;2.

——, L. Matrosova, C. Penland, J. D. Scott, and P. Chang, 2008: Forecasting Pacific SSTs: Linear inverse model predictions of the PDO. *J. Climate*, **21**, 385–402, https://doi.org/10.1175/2007JCLI1849.1.

Amaya, D. J., 2019: The Pacific meridional mode and ENSO: A review. *Curr. Climate Change Rep.*, **5**, 296–307, https://doi.org/10.1007/s40641-019-00142-x.

Angell, J. K., 2000: Tropospheric temperature variations adjusted for El Niño, 1958–1998. *J. Geophys. Res.*, **105**, 11 841–11 849, https://doi.org/10.1029/2000JD900044.

Balmaseda, M. A., K. Mogensen, and A. T. Weaver, 2013: Evaluation of the ECMWF ocean reanalysis system ORAS4. *Quart. J. Roy. Meteor. Soc.*, **139**, 1132–1161, https://doi.org/10.1002/qj.2063.

Barsugli, J. J., and P. D. Sardeshmukh, 2002: Global atmospheric sensitivity to tropical SST anomalies throughout the Indo-Pacific basin. *J. Climate*, **15**, 3427–3442, https://doi.org/10.1175/1520-0442(2002)015<3427:GASTTS>2.0.CO;2.

Bellenger, H., É. Guilyardi, J. Leloup, M. Lengaigne, and J. Vialard, 2014: ENSO representation in climate models: From CMIP3 to CMIP5. *Climate Dyn.*, **42**, 1999–2018, https://doi.org/10.1007/s00382-013-1783-z.

Bladé, I., M. Newman, M. A. Alexander, and J. D. Scott, 2008: The late fall extratropical response to ENSO: Sensitivity to coupling and convection in the tropical west Pacific. *J. Climate*, **21**, 6101–6118, https://doi.org/10.1175/2008JCLI1612.1.

Cane, M. A., A. C. Clement, A. Kaplan, Y. Kushnir, D. Pozdnyakov, R. Seager, S. E. Zebiak, and R. Murtugudde, 1997: Twentieth-century sea surface temperature trends. *Science*, **275**, 957–960, https://doi.org/10.1126/science.275.5302.957.

Capotondi, A., 2013: ENSO diversity in the NCAR CCSM4 climate model. *J. Geophys. Res. Oceans*, **118**, 4755–4770, https://doi.org/10.1002/jgrc.20335.

——, and P. D. Sardeshmukh, 2017: Is El Niño really changing? *Geophys. Res. Lett.*, **44**, 8548–8556, https://doi.org/10.1002/2017GL074515.

——, and Coauthors, 2015: Understanding ENSO diversity. *Bull. Amer. Meteor. Soc.*, **96**, 921–938, https://doi.org/10.1175/BAMS-D-13-00117.1.

——, P. D. Sardeshmukh, E. Di Lorenzo, A. Subramanian, and A. J. Miller, 2019: Predictability of US West Coast ocean temperatures is not solely due to ENSO. *Sci. Rep.*, **9**, 10993, https://doi.org/10.1038/s41598-019-47400-4.

——, A. T. Wittenberg, J. S. Kug, K. Takahashi, and M. J. McPhaden, 2020a: ENSO diversity. *El Niño Southern Oscillation in a Changing Climate, Geophys. Monogr.*, Vol. 253, Amer. Geophys Union, 65–86.

——, C. Deser, A. Phillips, Y. Okumura, and S. Larson, 2020b: ENSO and Pacific decadal variability in the Community Earth System Model version 2. *J. Adv. Model. Earth Syst.*, **12**, e2019MS002022, https://doi.org/10.1029/2019MS002022.

Ceballos, L. I., E. Di Lorenzo, C. D. Hoyos, N. Schneider, and B. Taguchi, 2009: North Pacific Gyre Oscillation synchronizes climate fluctuations in the eastern and western boundary systems. *J. Climate*, **22**, 5163–5174, https://doi.org/10.1175/2009JCLI2848.1.

Chelton, D. B., and R. E. Davis, 1982: Monthly mean sea-level variability along the west coast of North America. *J. Phys. Oceanogr.*, **12**, 757–784, https://doi.org/10.1175/1520-0485(1982)012<0757:MMSLVA>2.0.CO;2.

Chen, W., J. Feng, and R. Wu, 2013: Roles of ENSO and PDO in the link of the East Asian winter monsoon to the following summer monsoon. *J. Climate*, **26**, 622–635, https://doi.org/10.1175/JCLI-D-12-00021.1.

Chen, X., and J. M. Wallace, 2016: Orthogonal PDO and ENSO indices. *J. Climate*, **29**, 3883–3892, https://doi.org/10.1175/JCLI-D-15-0684.1.

——, and T. Zhou, 2018: Relative contributions of external SST forcing and internal atmospheric variability to July–August heat waves over the Yangtze River valley. *Climate Dyn.*, **51**, 4403–4419, https://doi.org/10.1007/s00382-017-3871-y.

Chiang, J. C. H., and D. J. Vimont, 2004: Analogous Pacific and Atlantic meridional modes of tropical atmosphere–ocean variability. *J. Climate*, **17**, 4143–4158, https://doi.org/10.1175/JCLI4953.1.

Chung, C. T. Y., S. B. Power, A. Sullivan, and F. Delage, 2019: The role of the South Pacific in modulating tropical Pacific variability. *Sci. Rep.*, **9**, 18311, https://doi.org/10.1038/s41598-019-52805-2.

Clarke, A. J., and S. Van Gorder, 1994: On ENSO coastal currents and sea levels. *J. Phys. Oceanogr.*, **24**, 661–680, https://doi.org/10.1175/1520-0485(1994)024<0661:OECCAS>2.0.CO;2.

Compo, G. P., and P. D. Sardeshmukh, 2009: Oceanic influences on recent continental warming. *Climate Dyn.*, **32**, 333–342, https://doi.org/10.1007/s00382-008-0448-9.

Deser, C., M. A. Alexander, and M. S. Timlin, 2003: Understanding the persistence of sea surface temperature anomalies in midlatitudes. *J. Climate*, **16**, 57–72, https://doi.org/10.1175/1520-0442(2003)016<0057:UTPOSS>2.0.CO;2.

——, ——, S.-P. Xie, and A. S. Phillips, 2010: Sea surface temperature variability: Patterns and mechanisms. *Annu. Rev.*

*Mar. Sci.*, **2**, 115–143, https://doi.org/10.1146/annurev-marine-120408-151453.

——, and Coauthors, 2012: ENSO and Pacific decadal variability in the Community Climate System Model version 4. *J. Climate*, **25**, 2622–2651, https://doi.org/10.1175/JCLI-D-11-00301.1.

——, I. R. Simpson, K. A. McKinnon, and A. S. Phillips, 2017: The Northern Hemisphere extratropical atmospheric circulation response to ENSO: How well do we know it and how do we evaluate models accordingly? *J. Climate*, **30**, 5059–5082, https://doi.org/10.1175/JCLI-D-16-0844.1.

——, ——, A. S. Phillips, and K. A. McKinnon, 2018: How well do we know ENSO's climate impacts over North America, and how do we evaluate models accordingly? *J. Climate*, **31**, 4991–5014, https://doi.org/10.1175/JCLI-D-17-0783.1.

Di Lorenzo, E., K. M. Cobb, J. C. Furtado, N. Schneider, B. T. Anderson, A. Bracco, M. A. Alexander, and D. J. Vimont, 2010: Central Pacific El Nino and decadal climate change in the North Pacific Ocean. *Nat. Geosci.*, **3**, 762–765, https://doi.org/10.1038/ngeo984.

Enfield, D. B., and J. S. Allen, 1980: On the structure and dynamics of monthly mean sea level anomalies along the Pacific coast of North and South America. *J. Phys. Oceanogr.*, **10**, 557–578, https://doi.org/10.1175/1520-0485(1980)010<0557:OTSADO>2.0.CO;2.

Eyring, V., S. Bony, G. A. Meehl, C. A. Senior, B. Stevens, R. J. Stouffer, and K. E. Taylor, 2016: Overview of the Coupled Model Intercomparison Project Phase 6 (CMIP6) experimental design and organization. *Geosci. Model Dev.*, **9**, 1937–1958, https://doi.org/10.5194/gmd-9-1937-2016.

Frankignoul, C., N. Sennéchael, Y. O. Kwon, and M. A. Alexander, 2011: Influence of the meridional shifts of the Kuroshio and the Oyashio Extensions on the atmospheric circulation. *J. Climate*, **24**, 762–777, https://doi.org/10.1175/2010JCLI3731.1.

——, G. Gastineau, and Y. O. Kwon, 2017: Estimation of the SST response to anthropogenic and external forcing and its impact on the Atlantic multidecadal oscillation and the Pacific decadal oscillation. *J. Climate*, **30**, 9871–9895, https://doi.org/10.1175/JCLI-D-17-0009.1.

Furtado, J. C., E. Di Lorenzo, N. Schneider, and N. A. Bond, 2011: North Pacific decadal variability and climate change in the IPCC AR4 models. *J. Climate*, **24**, 3049–3067, https://doi.org/10.1175/2010JCLI3584.1.

Henderson, S. A., D. J. Vimont, and M. Newman, 2020: The critical role of non-normality in partitioning tropical and extratropical contributions to PNA growth. *J. Climate*, **33**, 6273–6295, https://doi.org/10.1175/JCLI-D-19-0555.1.

Huang, B., and Coauthors, 2017: Extended Reconstructed Sea Surface Temperature, version 5 (ERSSTv5): Upgrades, validations, and intercomparisons. *J. Climate*, **30**, 8179–8205, https://doi.org/10.1175/JCLI-D-16-0836.1.

Joh, Y., and E. Di Lorenzo, 2019: Interactions between Kuroshio Extension and central tropical Pacific lead to preferred decadal-timescale oscillations in Pacific climate. *Sci. Rep.*, **9**, 13558, https://doi.org/10.1038/s41598-019-49927-y.

Jong, B. T., M. Ting, and R. Seager, 2021: Assessing ENSO summer teleconnections, impacts, and predictability in North America. *J. Climate*, **34**, 3629–3643, https://doi.org/10.1175/JCLI-D-20-0761.1.

Joseph, R., and S. Nigam, 2006: ENSO evolution and teleconnections in IPCC's twentieth-century climate simulations: Realistic representation? *J. Climate*, **19**, 4360–4377, https://doi.org/10.1175/JCLI3846.1.

Kao, H. Y., and J. Y. Yu, 2009: Contrasting eastern-Pacific and central-Pacific types of ENSO. *J. Climate*, **22**, 615–632, https://doi.org/10.1175/2008JCLI2309.1.

Kelly, P. M., and P. D. Jones, 1996: Removal of the El Niño–Southern Oscillation signal from the gridded surface air temperature data set. *J. Geophys. Res.*, **101**, 19 013–19 022, https://doi.org/10.1029/96JD01173.

Kucharski, F., and Coauthors, 2016: Atlantic forcing of Pacific decadal variability. *Climate Dyn.*, **46**, 2337–2351, https://doi.org/10.1007/s00382-015-2705-z.

Liguori, G., and E. Di Lorenzo, 2019: Separating the North and South Pacific meridional modes contributions to ENSO and tropical decadal variability. *Geophys. Res. Lett.*, **46**, 906–915, https://doi.org/10.1029/2018GL080320.

Liu, Z., and E. Di Lorenzo, 2018: Mechanisms and predictability of Pacific decadal variability. *Curr. Climate Change Rep.*, **4**, 128–144, https://doi.org/10.1007/s40641-018-0090-5.

——, L. Wu, R. Gallimore, and R. Jacob, 2002: Search for the origins of Pacific decadal climate variability. *Geophys. Res. Lett.*, **29**, 1404, https://doi.org/10.1029/2001GL013735.

McPhaden, M. J., and X. Yu, 1999: Equatorial waves and the 1997–98 El Niño. *Geophys. Res. Lett.*, **26**, 2961–2964, https://doi.org/10.1029/1999GL004901.

Monahan, A. H., J. C. Fyfe, M. H. P. Ambaum, D. B. Stephenson, and G. R. North, 2009: Empirical orthogonal functions: The medium is the message. *J. Climate*, **22**, 6501–6514, https://doi.org/10.1175/2009JCLI3062.1.

Moore, A. M., and R. Kleeman, 1996: The dynamics of error growth and predictability in a coupled model of ENSO. *Quart. J. Roy. Meteor. Soc.*, **122**, 1405–1446, https://doi.org/10.1002/qj.49712253409.

Newman, M., 2007: Interannual to decadal predictability of tropical and North Pacific sea surface temperatures. *J. Climate*, **20**, 2333–2356, https://doi.org/10.1175/JCLI4165.1.

——, G. P. Compo, and M. A. Alexander, 2003: ENSO-forced variability of the Pacific decadal oscillation. *J. Climate*, **16**, 3853–3857, https://doi.org/10.1175/1520-0442(2003)016<3853:EVOTPD>2.0.CO;2.

——, P. D. Sardeshmukh, and C. Penland, 2009: How important is air–sea coupling in ENSO and MJO evolution? *J. Climate*, **22**, 2958–2977, https://doi.org/10.1175/2008JCLI2659.1.

——, M. A. Alexander, and J. D. Scott, 2011: An empirical model of tropical ocean dynamics. *Climate Dyn.*, **37**, 1823–1841, https://doi.org/10.1007/s00382-011-1034-0.

——, and Coauthors, 2016: The Pacific decadal oscillation, revisited. *J. Climate*, **29**, 4399–4427, https://doi.org/10.1175/JCLI-D-15-0508.1.

Nidheesh, A. G., M. Lengaigne, J. Vialard, T. Izumo, A. S. Unnikrishnan, and C. Cassou, 2017: Influence of ENSO on the Pacific decadal oscillation in CMIP models. *Climate Dyn.*, **49**, 3309–3326, https://doi.org/10.1007/s00382-016-3514-8.

Niranjan Kumar, K., T. B. M. J. Ouarda, S. Sandeep, and R. S. Ajayamohan, 2016: Wintertime precipitation variability over the Arabian Peninsula and its relationship with ENSO in the CAM4 simulations. *Climate Dyn.*, **47**, 2443–2454, https://doi.org/10.1007/s00382-016-2973-2.

Patrick, L., and Coauthors, 2018: CERA-20C: A coupled reanalysis of the twentieth century. *J. Adv. Model. Earth Syst.*, **10**, 1172–1195, https://doi.org/10.1029/2018MS001273.

Pegion, K., C. M. Selman, S. Larson, J. C. Furtado, and E. J. Becker, 2020: The impact of the extratropics on ENSO diversity and predictability. *Climate Dyn.*, **54**, 4469–4484, https://doi.org/10.1007/s00382-020-05232-3.

Penland, C., 2019: The Nyquist issue in linear inverse modeling. *Mon. Wea. Rev.*, **147**, 1341–1349, https://doi.org/10.1175/MWR-D-18-0104.1.

——, and L. Matrosova, 1994: A balance condition for stochastic numerical models with application to the El Niño–Southern Oscillation. *J. Climate*, **7**, 1352–1372, https://doi.org/10.1175/1520-0442(1994)007<1352:ABCFSN>2.0.CO;2.

——, and P. D. Sardeshmukh, 1995: The optimal growth of tropical sea surface temperature anomalies. *J. Climate*, **8**, 1999–2024, https://doi.org/10.1175/1520-0442(1995)008<1999:TOGOTS>2.0.CO;2.

——, and L. Matrosova, 2006: Studies of El Niño and interdecadal variability in tropical sea surface temperatures using a non-normal filter. *J. Climate*, **19**, 5796–5815, https://doi.org/10.1175/JCLI3951.1.

Power, S., and Coauthors, 2021: Decadal climate variability in the tropical Pacific: Characteristics, causes, predictability and prospects. *Science*, **374**, eaay9165, https://doi.org/10.1126/science.aay9165.

Qiu, B., 2003: Kuroshio Extension variability and forcing of the Pacific decadal oscillations: Responses and potential feedback. *J. Phys. Oceanogr.*, **33**, 2465–2482, https://doi.org/10.1175/2459.1.

Rayner, N. A., D. E. Parker, E. B. Horton, C. K. Folland, L. V. Alexander, D. P. Rowell, E. C. Kent, and A. Kaplan, 2003: Global analyses of sea surface temperature, sea ice, and night marine air temperature since the late nineteenth century. *J. Geophys. Res.*, **108**, 4407, https://doi.org/10.1029/2002JD002670.

Robock, A., and J. Mao, 1995: The volcanic signal in surface temperature observations. *J. Climate*, **8**, 1086–1103, https://doi.org/10.1175/1520-0442(1995)008<1086:TVSIST>2.0.CO;2.

Rodríguez-Fonseca, B., I. Polo, J. García-Serrano, T. Losada, E. Mohino, C. R. Mechoso, and F. Kucharski, 2009: Are Atlantic Niños enhancing Pacific ENSO events in recent decades? *Geophys. Res. Lett.*, **36**, L20705, https://doi.org/10.1029/2009GL040048.

Sandeep, S., F. Stordal, P. D. Sardeshmukh, and G. P. Compo, 2014: Pacific Walker circulation variability in coupled and uncoupled climate models. *Climate Dyn.*, **43**, 103–117, https://doi.org/10.1007/s00382-014-2135-3.

Santer, B. D., and Coauthors, 2001: Accounting for the effects of volcanoes and ENSO in comparisons of modeled and observed temperature trends. *J. Geophys. Res.*, **106**, 28 033–28 059, https://doi.org/10.1029/2000JD000189.

Schneider, N., and B. D. Cornuelle, 2005: The forcing of the Pacific decadal oscillation. *J. Climate*, **18**, 4355–4373, https://doi.org/10.1175/JCLI3527.1.

Shin, S.-I., and M. Newman, 2021: Seasonal Predictability of global and North American coastal sea surface temperature and height anomalies. *Geophys. Res. Lett.*, **48**, e2020GL091886, https://doi.org/10.1029/2020GL091886.

Solomon, A., and Coauthors, 2011: Distinguishing the roles of natural and anthropogenically forced decadal climate variability: Implications for prediction. *Bull. Amer. Meteor. Soc.*, **92**, 141–156, https://doi.org/10.1175/2010BAMS2962.1.

Takahashi, K., A. Montecinos, K. Goubanova, and B. Dewitte, 2011: ENSO regimes: Reinterpreting the canonical and Modoki El Niño. *Geophys. Res. Lett.*, **38**, L10704, https://doi.org/10.1029/2011GL047364.

Thompson, D. W. J., J. J. Kennedy, J. M. Wallace, and P. D. Jones, 2008: A large discontinuity in the mid-twentieth century in observed global-mean surface temperature. *Nature*, **453**, 646–649, https://doi.org/10.1038/nature06982.

——, J. M. Wallace, P. D. Jones, and J. J. Kennedy, 2009: Identifying signatures of natural climate variability in time series of global-mean surface temperature: Methodology and insights. *J. Climate*, **22**, 6120–6141, https://doi.org/10.1175/2009JCLI3089.1.

Vimont, D. J., 2005: The contribution of the interannual ENSO cycle to the spatial pattern of decadal ENSO-like variability. *J. Climate*, **18**, 2080–2092, https://doi.org/10.1175/JCLI3365.1.

Vyushin, D., and P. J. Kushner, 2009: Power-law and long-memory characteristics of the atmospheric general circulation. *J. Climate*, **22**, 2890–2904, https://doi.org/10.1175/2008JCLI2528.1.

Wang, B., R. Wu, and X. Fu, 2000: Pacific–East Asian teleconnection: How does ENSO affect East Asian climate? *J. Climate*, **13**, 1517–1536, https://doi.org/10.1175/1520-0442(2000)013<1517:PEATHD>2.0.CO;2.

Wang, H., A. Kumar, W. Wang, and Y. Xue, 2012: Influence of ENSO on Pacific decadal variability: An analysis based on the NCEP Climate Forecast System. *J. Climate*, **25**, 6136–6151, https://doi.org/10.1175/JCLI-D-11-00573.1.

Wheeler, M. C., and H. H. Hendon, 2004: An all-season real-time multivariate MJO index: Development of an index for monitoring and prediction. *Mon. Wea. Rev.*, **132**, 1917–1932, https://doi.org/10.1175/1520-0493(2004)132<1917:AARMMI>2.0.CO;2.

Wills, R. C., T. Schneider, J. M. Wallace, D. S. Battisti, and D. L. Hartmann, 2018: Disentangling global warming, multidecadal variability, and El Niño in Pacific temperatures. *Geophys. Res. Lett.*, **45**, 2487–2496, https://doi.org/10.1002/2017GL076327.

Wu, L., C. Wang and B. Wang, 2015: Westward shift of western North Pacific tropical cyclogenesis. *Geophys. Res. Lett.*, **42**, 1537–1542, https://doi.org/10.1002/2015GL063450.

Yi, D. L., B. Gan, L. Wu, and A. J. Miller, 2018: The North Pacific Gyre Oscillation and mechanisms of its decadal variability in CMIP5 models. *J. Climate*, **31**, 2487–2509, https://doi.org/10.1175/JCLI-D-17-0344.1.

Yoon, J. H., and N. Zeng, 2010: An Atlantic influence on Amazon rainfall. *Climate Dyn.*, **34**, 249–264, https://doi.org/10.1007/s00382-009-0551-6.

You, Y., and J. C. Furtado, 2017: The role of South Pacific atmospheric variability in the development of different types of ENSO. *Geophys. Res. Lett.*, **44**, 7438–7446, https://doi.org/10.1002/2017GL073475.

Zhang, R. H., L. M. Rothstein, and A. J. Busalacchi, 1998: Origin of upper-ocean warming and El Niño change on decadal scales in the tropical Pacific Ocean. *Nature*, **391**, 879–883, https://doi.org/10.1038/36081.

Zhang, Y., J. M. Wallace, and D. S. Battisti, 1997: ENSO-like interdecadal variability: 1900–93. *J. Climate*, **10**, 1004–1020, https://doi.org/10.1175/1520-0442(1997)010<1004:ELIV>2.0.CO;2.

——, S. Xie, Y. Kosaka, and J. Yang, 2018: Pacific decadal oscillation: Tropical Pacific forcing versus internal variability. *J. Climate*, **31**, 8265–8279, https://doi.org/10.1175/JCLI-D-18-0164.1.

Zhao, J., J.-S. Kug, J.-H. Park, and S.-I. An, 2020: Diversity of North Pacific meridional mode and its distinct impacts on El Niño–Southern Oscillation. *Geophys. Res. Lett.*, **47**, e2020GL088993, https://doi.org/10.1029/2020GL088993.

Zhao, Y., and E. Di Lorenzo, 2020: The impacts of extra-tropical ENSO precursors on tropical Pacific decadal-scale variability. *Sci. Rep.*, **10**, 3031, https://doi.org/10.1038/s41598-020-59253-3.

——, ——, D. Sun, and S. Stevenson, 2021: Tropical Pacific decadal variability and ENSO precursor in CMIP5 models. *J. Climate*, **34**, 1023–1045, https://doi.org/10.1175/JCLI-D-20-0158.1.